Sensitivity of Monthly Three-Dimensional Radar-Echo Characteristics to Sampling Frequency

By Matthias Steiner[1] and Robert A. Houze Jr.

Department of Atmospheric Sciences, University of Washington, Seattle, Washington

(Manuscript received 21 April 1997, in revised form 20 November 1997)

Abstract

Estimates of any precipitation characteristics based on temporally sparse observations entail uncertainty because of the natural variability of rainfall in space and time. This study measures the sampling-related uncertainties of monthly mean reflectivity profile and surface rainfall distribution. Radar and rain gauge data collected during the 1993/94 monsoon season at Darwin, Australia, are used to show the sensitivity of monthly three-dimensional radar-echo and precipitation characteristics to the frequency of observation. The data are partitioned into convective, stratiform, and anvil components according to the horizontal and vertical structure of the echoes. The analyses of this study reveal the expected trend that the uncertainties of estimated precipitation characteristics using infrequent observations scale with rainfall amount. The results have implications for climatological studies using spaceborne observation platforms revisiting a given area intermittently.

The Tropical Rainfall Measuring Mission (TRMM) satellite radar, which will revisit a given 500 km by 500 km region approximately twice daily, will likely encounter significant problems in estimating the vertical profile of radar reflectivity in the tropics. Monthly mean reflectivity statistics (based on observations within 150 km of the Darwin radar) exhibit a sampling-related uncertainty of about 20 % in both rain and snow. In addition, the radar signal of the TRMM satellite will be highly attenuated below the 0°C level, and the precipitation radar will be insensitive to reflectivity less than about 20 dBZ. Therefore, the spaceborne radar will have an obscured view of the vertical precipitation structure. Reliable reflectivity statistics based on TRMM satellite radar data may be obtained primarily within an altitude range of about 5–7.5 km—an altitude range though that is important for cloud electrification because of the mixed-phase precipitation processes taking place there. The sampling uncertainty, signal attenuation, and radar sensitivity vary with precipitation type. Moreover, estimation of the convective rain fraction will be compromised by uncertainties in the echo classification as well as a choice of $Z - R$ relation. These results imply the importance of information collected by ground validation site radars to improve upon TRMM satellite estimates of precipitation characteristics and the derived vertical profile of latent heating.

1. Introduction

Estimates of precipitation characteristics on a climatological time scale based on temporally sparse observations exhibit uncertainty, which is a function of the rainfall variability in space and time. A key question is, how often do we have to make observations to describe monthly precipitation characteristics accurately? The answer is critical to the Tropical Rainfall Measuring Mission (TRMM; Simpson *et al.*, 1988, 1996), which will use spaceborne radar and other instrumentation to observe precipitation on a global scale continuously for several years, beginning with the launch of the satellite late in 1997.

TRMM will emphasize measures of monthly quantities over regions approximately 500 km in horizontal dimension. These quantities include vertical profiles of radar reflectivity and surface rainfall amount. Moreover, algorithms will subdivide the data into convective and stratiform components. This study uses radar and rain gauge data collected during the 1993/94 wet season at Darwin, Australia, to determine the effect of discrete temporal sampling on the estimation of these monthly quantities. We do not consider partial visits and assume therefore that the region of interest is fully sampled each time the satellite passes over.

1 Corresponding author: Dr. Matthias Steiner, Dept. of Civil Engineering and Operations Research, Princeton University, Princeton, NJ 08544. Phone: 609/258-4614, Fax: 609/258-2799, E-mail: msteiner@radap.princeton.edu

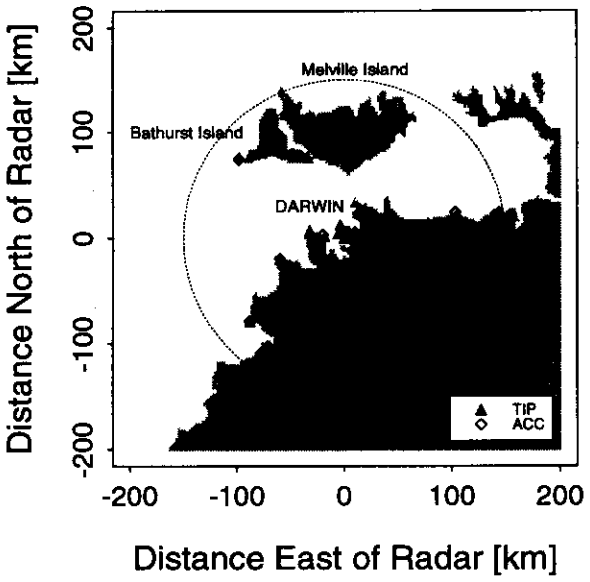

Fig. 1. Geographical map of the Darwin area, centered on the radar installation at Berrimah (12° 27' 26" S and 130° 55' 31" E). The rain gauge network is shown by the bold triangles and open diamonds, indicating the location of the tipping-bucket (TIP) and accumulation (ACC) gauges, respectively. The dotted circle (radius of 150 km) embraces the study domain.

2. Methodology and data

2.1 Site description and data processing

Darwin lies just south of Indonesia and Malaysia (the "maritime continent"; Ramage, 1968). The region experiences a monsoonal climate, with a rainy season usually extending from late December through March (Holland, 1986; Keenan *et al.*, 1988; Drosdowsky, 1996). The precipitation observed by the Darwin radar is of three main types (*e.g.*, Keenan and Carbone, 1992): 1) During active monsoon periods (low-level westerly winds), precipitation is produced largely by oceanic mesoscale convective systems (Mapes and Houze, 1992, 1993). 2) During breaks in the monsoon (low-level easterlies), precipitating cloud systems are less frequent and typically of a continental origin. They may be intense and often form squall lines with trailing stratiform precipitation (Drosdowsky, 1984). 3) Pronounced diurnally forced thunderstorms, locally known as "Hectors" (Keenan *et al.*, 1989a, 1990; Simpson *et al.*, 1993), occur over Bathurst and Melville Islands to the north of Darwin (Fig. 1).

In 1993/94, the Darwin radar was operated by the Australian Bureau of Meteorology Research Centre (BMRC), and had a wavelength of 5 cm and a beamwidth of 1°. It was located at Berrimah (12° 27' 26" S and 130° 55' 31" E), about 20 km east-southeast of Darwin. The radar site was 30 m above mean sea level (MSL).[2] The surrounding rain gauge network, also operated by BMRC, consisted of 20–30 tipping-buckets and another 25–30 accumulation rain gauges (Fig. 1). Further details about the network can be found in Keenan *et al.* (1988), Rosenfeld *et al.* (1993), Short *et al.* (1993), Steiner *et al.* (1995), and Steiner (1996).

Radar volume scans were recorded every 10 min. We grouped the data into two "monthly" time periods: The first period consists of 25 days of radar information of December 1993 and January 1994 (Table 1); the second period has 20 days of data collected in February and March 1994 (Table 2). Only days with almost complete records (*i.e.*, less than 10 % of radar volumes missing per day) are used for this analysis to avoid the introduction of additional uncertainty due to data gaps. Since the selected periods are shorter than 30 days, the magnitude of uncertainties derived in our study are somewhat higher than those of a full month. The uncertainties for a complete month would roughly be scaled by a factor corresponding to the square root of the ratio of the number of days in the sample divided by 30 days (*e.g.*, Bell *et al.*, 1990; Steiner, 1996).

For this study, each radar volume is interpolated to a three-dimensional Cartesian grid with a resolution of 2 km in the horizontal and 1.5 km in the vertical. The domain is centered on the Darwin radar and has a horizontal extent of 300 km by 300 km.[3] The levels in the vertical are 1.5 km to 19.5 km above ground. Bilinear interpolation determines the radar reflectivity value at the grid points by means of the Sorted Position Radar Interpolation software (SPRINT; Mohr and Vaughan, 1979),[4] a software package maintained by the National Center for Atmospheric Research (NCAR).

The radar reflectivity echo pattern at the lowest (0.5 degree) elevation sweep is separated into convective and stratiform elements using the method described by Steiner *et al.* (1995). This technique searches for convective precipitation and lets the remainder be stratiform. The basic premise is that the signature of convective precipitation is readily identifiable in the intensity and peakedness[5] of the horizontal patterns of reflectivity, while stratiform precipitation is often not easily recognizable

2 All heights given in this paper are relative to the mean sea level (MSL).

3 Similarly to the scaling in time, the sampling-related uncertainties obtained on the radar-covered domain have to be scaled to a 500 km by 500 km domain for TRMM.

4 SPRINT is available from the NCAR Mesoscale and Microscale Meteorology (MMM) Division. Please contact William D. Anderson (email: andersnb@ncar.ucar.edu) or L. Jay Miller (email: ljmill@ncar.ucar.edu).

5 Peakedness is not to be confused with gradients of precipitation. Peakedness is more similar to the Laplacian of the reflectivity field than to the gradient in that we search for maxima of a certain intensity and/or steepness.

Table 1. Daily areal rainfall information for time period 1 based on radar and rain gauge data collected during the 1993/94 monsoon season at Darwin, Australia. The rainfall amounts are computed from the radar data using a gauge-adjusted reflectivity–rainfall rate relationship. A 24 h period following 0000 UTC is used for deriving the daily amounts. The areal mean rainfall accumulation represents an average rainfall depth over a circular domain with radius of 150 km centered on the Darwin radar installation. The convective rain fraction gives the percentage of the areal rainfall that is contributed by convective precipitation radar echoes (see text for details). The last column indicates the number of radar volume scans per day that entered the analysis.

Date	*Areal Rain* [mm]	*Conv Fraction* [%]	*Radar Volumes*
93/12/24	3.98	72.61	141
93/12/25	14.01	53.53	141
93/12/26	19.68	53.66	141
93/12/28	33.69	27.49	144
93/12/29	6.93	25.83	140
93/12/30	22.78	44.51	141
93/12/31	2.28	50.88	133
94/01/01	7.44	63.04	143
94/01/02	2.47	66.40	139
94/01/03	0.35	74.29	143
94/01/04	23.00	33.30	132
94/01/05	0.54	7.41	144
94/01/06	1.15	75.65	143
94/01/07	14.82	58.10	136
94/01/08	4.01	41.90	141
94/01/09	3.78	69.84	142
94/01/10	7.69	64.24	136
94/01/11	17.74	50.23	140
94/01/12	5.66	55.65	138
94/01/18	9.04	78.10	142
94/01/19	9.68	75.31	141
94/01/20	3.76	80.85	142
94/01/21	19.73	56.77	139
94/01/22	0.84	84.52	144
94/01/23	10.99	65.15	140
Total	245.35	50.74	3506

in either horizontal or vertical distributions of reflectivity. This method has been thoroughly tested by Steiner *et al.* (1995) and found to produce results that are consistent with the physical understanding of convective and stratiform precipitation (Houghton, 1968; Houze, 1993, 1997). Any radar echo aloft with no echo at the lowest elevation scan is called anvil. Figure 2 illustrates schematically how a radar volume is subdivided into convective, stratiform, and anvil echoes.

The radar rainfall estimates are calibrated using the rain gauge data. A single power-law relationship, $Z = \alpha R^{\beta}$, is used to convert radar reflectivity Z to rainfall rate R on a pixel by pixel basis at the lowest level. Starting with the GATE[6] $Z - R$ relation ($\alpha = 230$, $\beta = 1.25$; Austin *et al.*, 1976; Hudlow, 1979), the multiplicative factor α is tuned such that the mean bias of the radar rainfall estimates within small windows (*i.e.*, closest pixel) at the rain gauge sites is removed on a monthly basis. The resulting $Z - R$ relationships are

$$Z = \begin{cases} 77R^{1.25} \text{ (period 1)} \\ 86R^{1.25} \text{ (period 2)} \end{cases} \quad (1)$$

These $Z - R$ relations are in close agreement with the one determined by Williams *et al.* (1992) for rainfall observed during the Down Under Doppler and Electricity Experiment (DUNDEE; Rutledge *et al.*, 1992) in the vicinity of Darwin.

2.2 Methodology for analyzing the uncertainty as a function of sampling frequency

The uncertainty in a monthly analysis of the three-dimensional structure of radar echoes depends on how many volume scans enter the analysis. To determine this uncertainty, we subsample the available radar data at various time intervals. We use only volumes collected at, say 30 min apart (every third volume), to determine the quantities of interest and compare that result with the one obtained by using every available radar volume of a given time

6 GARP (Global Atmospheric Research Program) Atlantic Tropical Experiment. Its field phase was in 1974.

Table 2. Daily areal rainfall information for period 2, similarly to Table 1.

Date	*Areal Rain* [mm]	*Conv Fraction* [%]	*Radar Volumes*
94/02/10	4.11	82.97	143
94/02/14	21.98	58.87	140
94/02/15	24.75	47.96	144
94/02/16	24.57	49.49	143
94/02/17	25.58	48.12	144
94/02/18	9.42	60.08	130
94/02/21	21.47	64.97	140
94/02/24	12.22	43.62	128
94/02/25	21.37	39.35	144
94/02/27	32.16	42.57	144
94/02/28	31.51	44.11	144
94/03/01	32.74	37.97	144
94/03/03	8.86	58.35	135
94/03/04	10.55	53.46	144
94/03/05	6.54	68.35	131
94/03/07	10.21	69.05	144
94/03/08	13.48	53.26	144
94/03/09	23.51	37.30	144
94/03/10	17.62	40.18	144
94/03/11	18.13	44.07	144
Total	374.02	48.27	2818

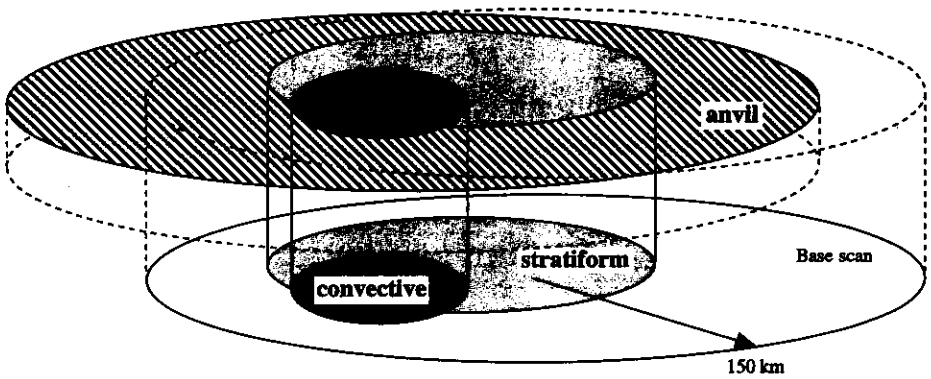

Fig. 2. Schematic visualization of the classification of radar echoes into convective and stratiform elements, and anvil (no surface rainfall). The precipitation echoes are classified according to their radar signatures at low levels and the echoes within a vertical column aloft are classified the same as the low-level pixel. Any radar echo aloft and outside the convective and stratiform vertical columns is assumed to be anvil. Thus, the vertical projection of anvil echo pixels fall outside the area identified as surface rainfall. Together with a land-ocean separation (not shown), the radar echoes may be grouped into twelve different categories and subcategories: total, total-land, total-ocean; convective, convective-land, convective-ocean; stratiform, stratiform-land, stratiform-ocean; anvil, anvil-land, and anvil-ocean.

period. We consider sampling intervals of 10 min (= full resolution), 20 min, 30 min, 1 h, 2 h, 3 h, 4 h, 6 h, 8 h, 12 h, and 24 h (= one volume a day). For each sampling frequency, we estimate the monthly result for every possible realization. For example, using a 30 min time interval, one could take the first sample at 0010, 0020, or 0030 UTC and include subsequent radar volumes 30 min apart. Our procedure is to make a separate calculation for each possible starting time (realization). The uncertainty for a given sampling frequency is then determined as the standard deviation of the ensemble of differences obtained by subtracting a subsampled result from the full resolution result. Steiner *et al.* (1995) and Steiner (1996) used similar procedures.

To compute monthly precipitation characteristics based on subsampled radar volumes, we assume that the information in a given volume represents the time interval in between two samples and that each volume has equal weight. Because

of range-dependent problems intrinsic to radar observations (Donaldson, 1964; Wilson and Brandes, 1979; Zawadzki, 1984; Austin, 1987; Joss and Waldvogel, 1990; Smith, 1990; Fabry *et al.*, 1992; Rosenfeld *et al.*, 1992; Kitchen and Jackson, 1993; Smith *et al.*, 1996), we only use the information contained within a horizontal range of 150 km.

2.3 Precipitation characteristics revealed by the radar data

The rainfall accumulations within 150 km of the Darwin radar for the two quasi-monthly periods are shown in Fig. 3. The areal mean rainfall totaled 245 mm for the first (Fig. 3a, Table 1) and 374 mm for the second time period (Fig. 3b, Table 2). Daily average accumulations over the 150 km radius domain range from essentially no rain to more than 30 mm. The contributions made by convective rainfall range from 7 % on 5 January 1994 to 85 % on 22 January 1994 (Tables 1 and 2). Days with a convective rain fraction of at least 65 % show areal mean rainfall accumulations of less than 10 mm (Fig. 4). Such rainfall typically originated from intense island thunderstorms and infrequent isolated continental convection and occurred during breaks in the monsoon (Troup, 1961; Holland, 1986; Drosdowsky, 1996). Most days, however, exhibited convective rain fractions of approximately 30 %–60 %, which are typical for tropical mesoscale convective systems (Houze, 1977; Cheng and Houze, 1979; Gamache and Houze, 1983; Leary, 1984; Churchill and Houze, 1984; Houze and Rappaport, 1984; Wei and Houze, 1987; Chong and Hauser, 1989; Gage *et al.*, 1994; Steiner *et al.*, 1995; and others). Continental squall lines tend to fall under this category as well. For example, a squall line moving across the domain on 4 January 1994 produced an areal mean rainfall accumulation of 23 mm of which 33 % was convective. Generally, the convective rain fraction decreased with increasing daily rainfall amount, as indicated by Fig. 4. Exceptions to that were 29 December 1993 and 5 January 1994, both affected by the remnants of a major rainfall event the previous day, the former by a very active monsoon spell and the latter by a major continental squall line. Days with a significant areal mean rainfall amount dominated the overall rainfall accumulation for a given time period as well as the convective rain fraction thereof (Tables 1 and 2).

As in Steiner *et al.* (1995), we determined the fraction of the radar-observed domain covered by precipitation echo for each individual radar volume. The height of each bar in Fig. 5 shows the closest-to-the-ground net area coverage (upper panels) and rain amount (lower panels), respectively, contributed by all the individual volumes in that category combined and normalized to the monthly total for both periods. In addition, the plots show the cumulative distributions of the accumulated area and rain, respectively, and the fractional contributions made by convective and stratiform precipitation echoes. These statistics do not include area covered by anvil echoes aloft, which, by definition, have no surface rainfall.

The echo area coverage distributions differ between periods 1 (Fig. 5a) and 2 (Fig. 5b) such that the distribution for period 1 is wide (maximum area coverage was 85 %–90 % observed on 28 December 1993) and shows significant contributions made from radar volumes with smaller echo area coverages. The distribution for time period 2, on the other hand, has the most contributions made by radar echoes covering up 20 %–50 % of the domain. Sixteen out of the 25 days (*i.e.*, 64 %) of period 1 have area-average rainfall amounts < 10 mm (Table 1), characteristic of monsoon break periods. The significant contributions made by echo areas covering less than 20 % of the radar domain are largely the result of the Hectors. In contrast to period 1, only 20 % of the days of period 2 exhibited less than 10 mm of rainfall (Table 2). The distribution shown in Fig. 5b represents a period of active monsoon rainfall. Despite the differences in break versus monsoonal regimes, the two time periods were similar in terms of the overall convective contribution to total echo area coverage (Figs. 5a and 5b)—in both periods the majority of the radar echoes ($\sim$ 90 % by area) are of stratiform nature.

The statistics with regard to the monthly areal rainfall contribution (Figs. 5c and 5d) made by radar echoes covering different proportions of the domain are similar to Figs. 5a and 5b. However, the rainfall contributed by smaller precipitation systems for period 1 is more pronounced in Fig. 5c than the area statistic shown in Fig. 5a, primarily because of the high rain rates observed in the island thunderstorms to the north of Darwin. Occasional Hectors observed during the few break days of period 2 contributed a secondary peak in the distribution at 5 %–10 % area coverage (Fig. 5d). Both periods show similarity again in convective and stratiform rainfall contributions to the monthly total (Figs. 5c and 5d)—the rainfall amounts contributed by the two physically distinct types of precipitation are about equal ($\sim$ 50 %).

3. Vertical distribution of radar reflectivity

The vertical distribution of radar reflectivity is a measure of the vertical distribution of precipitation hydrometeors. Though there is no one-to-one relationship between where the precipitation-sized hydrometeors are observed and where the latent heat has actually been released by condensation or vapor deposition, reflectivity may be used as a constraint for model estimation of the latent heat released to the atmosphere. In addition, comparison between the TRMM satellite precipitation radar data and

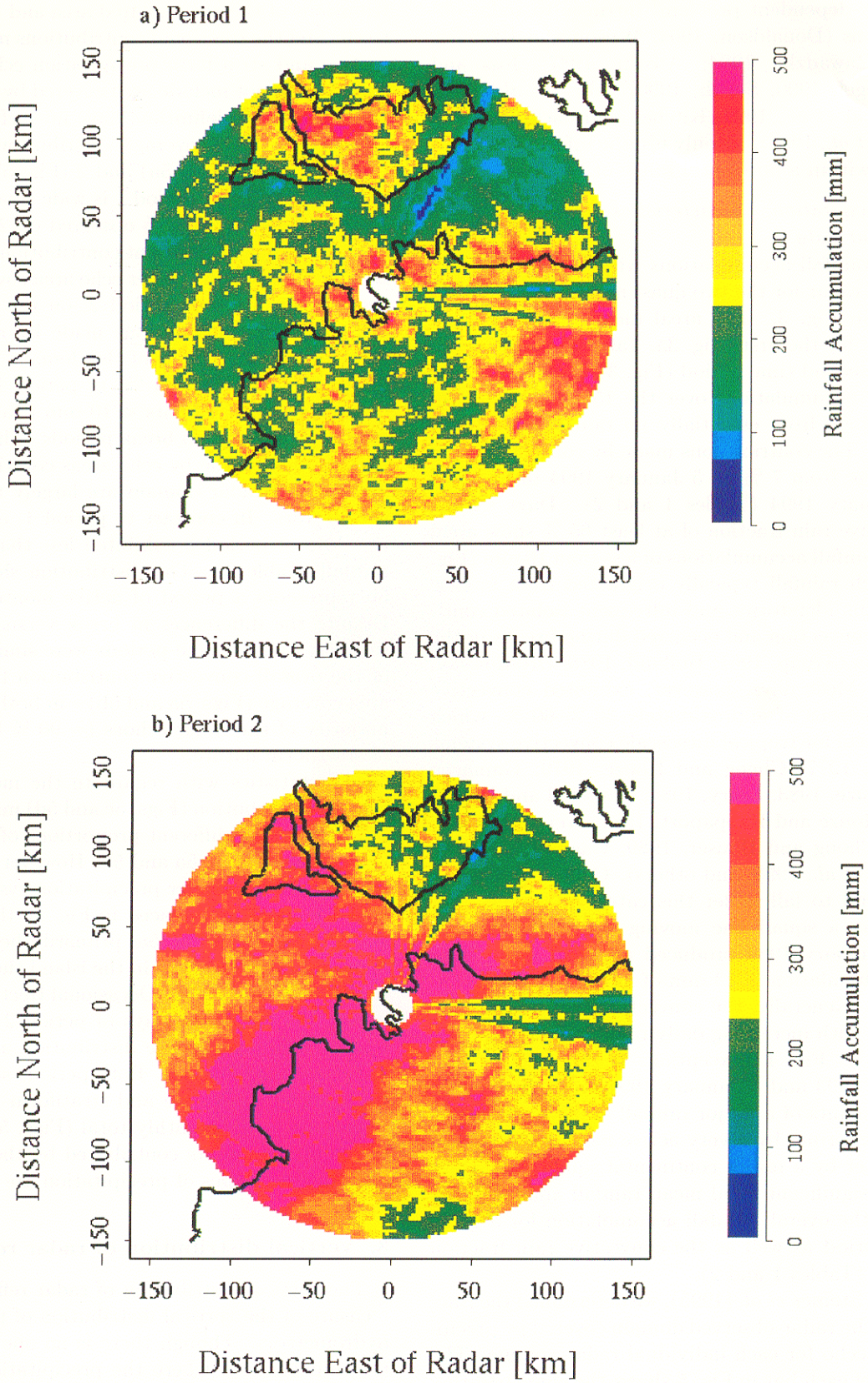

Fig. 3. Rainfall accumulation maps for Darwin, Australia. The rainfall amounts are computed using the gauge-adjusted reflectivity-rainfall rate relationships as shown in the text. The black contours indicate the coastlines around Darwin. a) period 1 (December 1993–January 1994) and b) period 2 (February–March 1994).

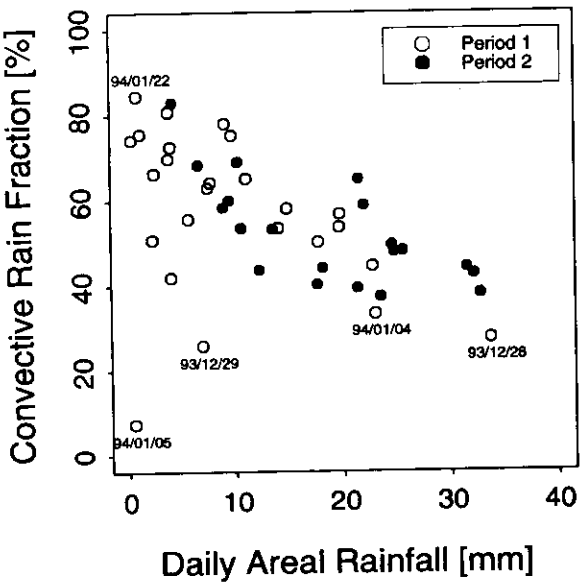

Fig. 4. Convective rain fractions as a function of the daily areal rainfall amount for precipitation observed during the rainy season 1993–94 at Darwin, Australia. See text for details.

data collected by radars at ground validation sites will be based on three-dimensional reflectivity information. It is important, therefore, to focus on the vertical distribution of reflectivity, but also on the effects of sampling limitations on the observed structures.

3.1 Contoured Frequency by Altitude Diagram and mean profiles

The Contoured Frequency by Altitude Diagram (CFAD; Yuter and Houze, 1995) is a useful method to summarize the information contained in three-dimensional radar volume scans. The CFAD is a contoured representation of the frequency of occurrence of radar reflectivity values as a function of height. The reflectivity CFADs for periods 1 and 2 are presented in Figs. 6 and 7. At first glance, the distributions shown for the different categories of radar echoes are very similar for the two periods analyzed. The convective and stratiform CFADs indicate a general decrease of reflectivity with increasing height, particularly above the freezing level ($\sim$ 4.5 km), while the anvil CFAD shows no such trend. Yuter and Houze (1995) noted that the reflectivities tend to be narrowly distributed in stratiform precipitation, while convection—especially in early stages—shows wider reflectivity distributions. Overlaying the CFADs for periods 1 and 2 (Figs. 6 and 7) shows that the modes of the distributions are very similar. However, there are a few noteworthy differences: The convective reflectivity distribution at low levels (below the melting layer) is very similar between the two time periods. But at higher levels the convective reflectivity distribution of period 1 is significantly wider than that of period 2. The more intense reflectivities at higher levels are contributed by the more vigorous continental and island convection (incorporating stronger updrafts, which can carry large particles to higher altitudes), which were more frequently observed during period 1 than 2. This is also reflected in the mean profiles[7] shown in Fig. 8. The average reflectivity decrease with increasing height of the convective radar echoes of period 1 is approximately -2.5 dBZ km^{-1} in the range of 5–9 km in altitude (0°C to -20°C) compared to maybe -3.5 dBZ km^{-1} for period 2. The stratiform reflectivity distributions are more similar between the two time periods, though the mean profile of period 1 has somewhat larger intensities at higher altitudes (Fig. 8). The average reflectivity decrease with increasing height for the stratiform radar echoes is approximately -4.5 dBZ km^{-1} within a 2 km layer above the melting layer and less further aloft. The reflectivity distributions and the mean profiles of the anvil echoes consist of weak echoes (< 20 dBZ) with no significant vertical structure.

Although anvil echoes do not contribute to surface rainfall, they occupy significant portions of the three-dimensional radar echo volume. The lowest level (1.5 km) contains by definition no anvil echoes (Section 2.1); at that level about 10 % of the radar echo pixels were classified as convective and the remaining 90 % as stratiform for the two time periods studied (Fig. 5). Further aloft, convective echoes contributed about 5 %–10 % to the echo area at each atltitude level, while the remaining echoes were about equally divided among stratiform and anvil echoes (varying between 35 % and 60 %). Though not explicitly shown, this may be seen from Figs. 6 and 7.

3.2 Accuracy of mean profiles of radar reflectivity

Figure 9 illustrates the uncertainty in the monthly mean vertical reflectivity profile as a result of intermittent sampling frequency (Δt = 1, 3, 6, 12 h). Fig. 9a shows the six different estimates of the monthly mean vertical reflectivity profile for convective echoes obtained by using only the radar volumes collected one hour apart, starting at 0000, 0010, 0020, 0030, 0040, or 0050 UTC, respectively. To the left of the mean profiles, the standard deviation of the different mean profile reflectivity values obtained at each altitude is indicated. It is noteworthy to point out that the variability of the mean profile estimates, as indicated by the standard deviation, is due to a combination of physical reasons (growth and decay of storm systems, diurnal cycle of precipitation) and sampling. However, we do not attempt to make such a distinction and thus treat the ob-

7 The mean profiles were obtained by averaging reflectivity values in mm^6 m^{-3} at each height level.

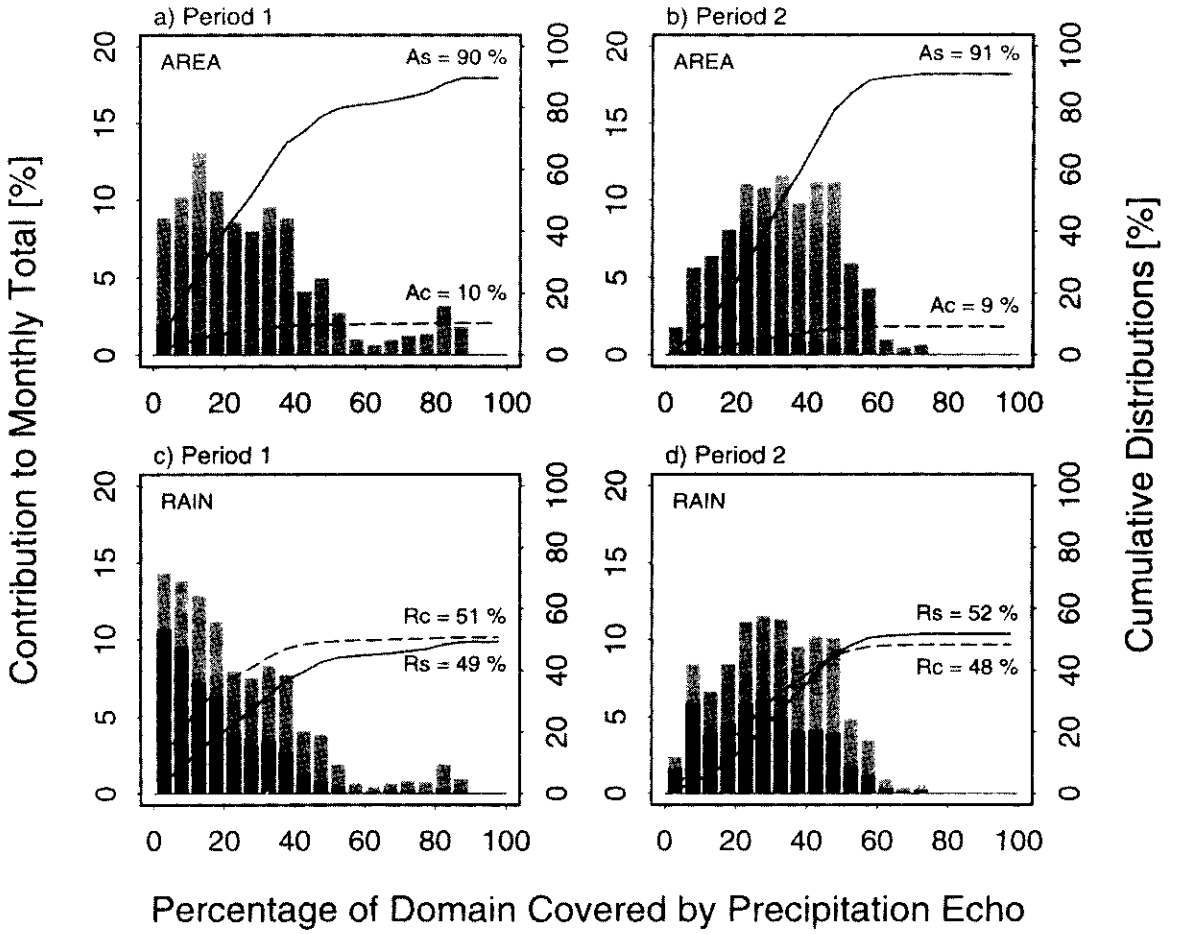

Fig. 5. Echo area (upper panels) and rainfall statistics (lower panels) as a function of the domain covered by precipitating echoes for the ensemble of individual radar volumes. The analyses for period 1 are shown to the left and those for period 2 to the right. For the bar graph, the abscissa indicates the percentage of the domain covered by precipitation echoes, while the ordinate on the lefthand side of each panel indicates the contribution to the monthly echo area (upper panels) and rainfall accumulation (lower panels). The dark (light) shading shows the convective (stratiform) contribution to each bar. In the upper panels, the dashed (solid) curve shows the cumulative area covered by convective (stratiform) echoes. Ac (As) is the total area covered by convective (stratiform) echo during a particular period. Similarly, in the lower panels the cumulative curves for the rainfall accumulation are indicated, where Rc (Rs) is the total rain from convective (stratiform) echo during that period.

served variability as being entirely due to sampling. For most parts of the monthly mean profile, especially in the rain below the melting layer at about 4.5 km, the different estimates of the monthly profile are barely distinguishable. Even with a sampling frequency of $\Delta t = 3$ h (Fig. 9b), the different profile estimates follow each other closely. The variability at upper levels becomes more noticeable at $\Delta t = 6$ h (Fig. 9c) and quite large at $\Delta t = 12$ h (Fig. 9d). The latter corresponds roughly to the sampling frequency of the TRMM satellite. However, despite the few radar volumes entering the computation of a mean profile at $\Delta t = 12$ h sampling frequencies, the standard deviation of the estimated mean reflectivity at lower levels is not very large (< 1 dBZ below 6 km).

Thus, in principle, the TRMM satellite will sample the radar reflectivity often enough to obtain, on average, an accurate vertical profile below the 0°C level. However, the wavelength of the TRMM satellite radar is only 2 cm and the received signals will therefore be highly attenuated through and below the melting layer. The vertical reflectivity profile measured by the satellite will thus not directly be useful below an altitude of maybe 5 km (Fig. 9d). Another limitation of the TRMM satellite radar is its low sensitivity—*i.e.*, the minimum detectable reflectivity is approximately 20 dBZ. With this additional shortcoming, it is evident from Fig. 9d that the TRMM satellite will obtain a completely unat-

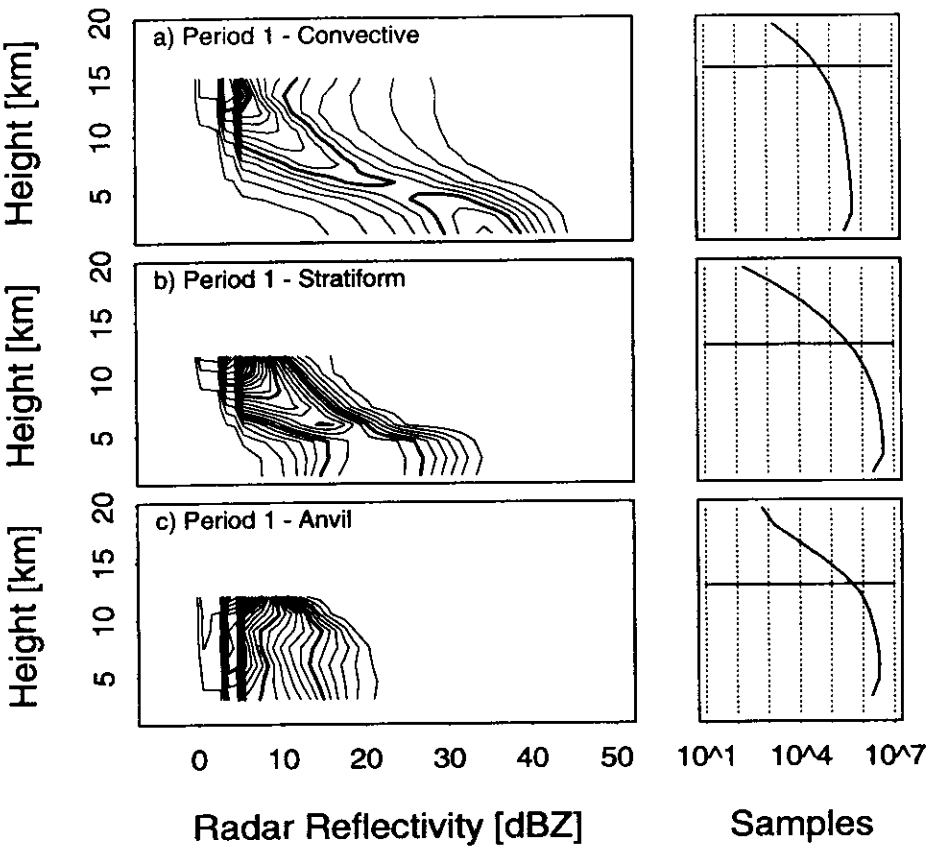

Fig. 6. Contoured Frequency by Altitude Diagrams (CFAD) for radar reflectivity volumes collected during period 1, subdivided into a) convective, b) stratiform, and c) anvil echoes. The resolution is 1 dBZ in reflectivity and 1.5 km in height. The contours are at intervals of 0.5 % of data per dBZ per kilometer, starting with the 0.5 % dBZ^{-1} km^{-1} contour and every 6th contour is highlighted. The CFADs are truncated at the altitude where the total number of points (per height level) drops below 15 % of the maximum number of points at any level, as indicated in the panels to the right.

tenuated sample of reflectivity only in the layer between about 5 and 7.5 km. Interestingly though, this is the layer where mixed-phase precipitation processes take place which are important for cloud electrification.

Though there are differences in the vertical distribution of reflectivity between convective and stratiform precipitation, and anvil echoes, the above caveats are generally true for all types of precipitation to be observed by the TRMM satellite radar. More specifically, Fig. 8 indicates that for convective precipitation the echoes seen aloft will likely be strong enough to be seen by the TRMM satellite radar, though attenuation of the signal will increase towards lower levels and be particularly strong below the 0°C level in the rain—possibly severe enough that no measurements will be obtained down to the surface. In stratiform precipitation some of the echoes aloft might not be seen by the spaceborne radar due to instrument sensitivity limitations and attenuation through the bright band (*i.e.*, melting layer) and below in the rain may again weaken the signal (though less than in convective rainfall). Anvil echoes will be completely missed by the TRMM satellite radar. In short, the spaceborne radar will get an obscured picture of the vertical precipitation structure. This emphasizes therefore that classification algorithms based on TRMM satellite radar data should not rely on vertical structure information alone but also make use of horizontal information contained in the swath.

Figure 10a compiles the information contained in Fig. 9 with the results of other sampling frequencies. The symbols show that the standard deviation of monthly mean convective reflectivity values increases with increasing altitude and decreasing sampling frequency. The uncertainty of the monthly mean reflectivity profile increases more rapidly with decreasing frequency of observations above the 0°C level ($\sim$ 4.5 km) than within the rain. This increased uncertainty aloft may in part also be caused by the decreasing number of data with increasing altitude, as shown in Figs. 6 and 7. The uncertainties tend to be larger for the convective mean profiles (Fig. 10a) than those composed of stratiform echoes (Fig. 10b), but smaller than for the

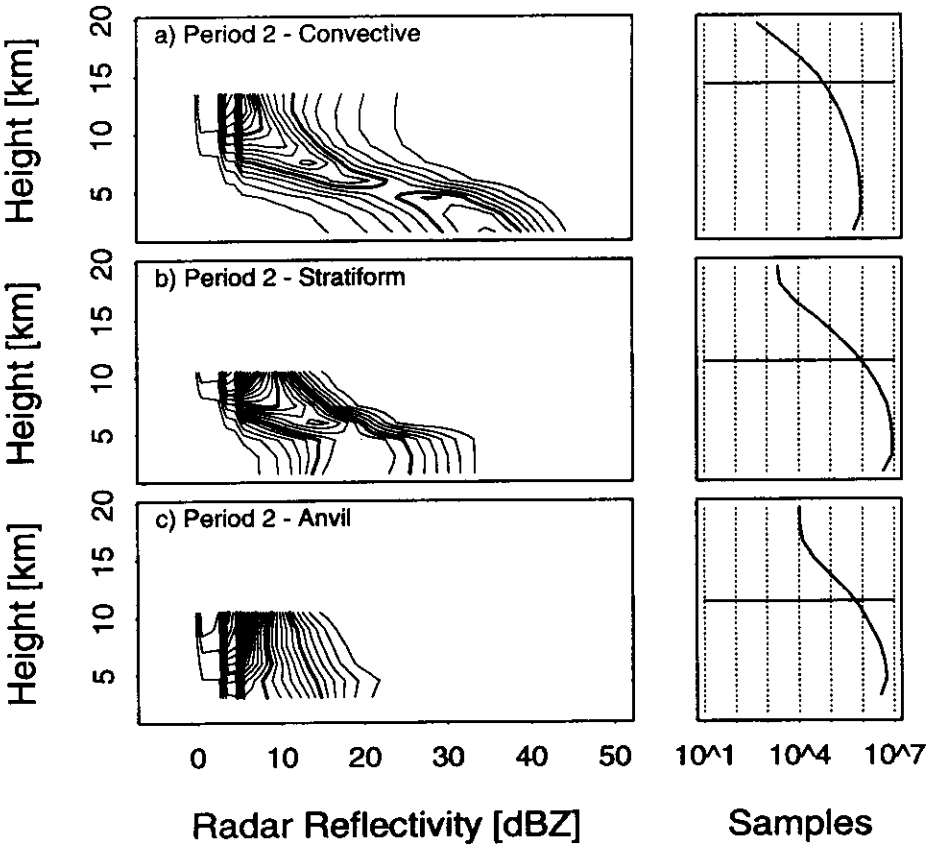

Fig. 7. Same as Fig. 6, but for period 2.

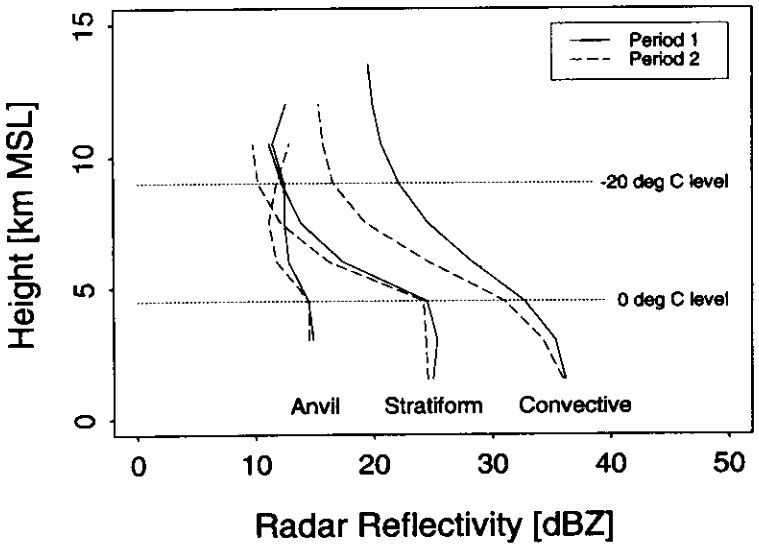

Fig. 8. Mean profiles of radar reflectivity volumes collected during period 1 (solid lines) and period 2 (dashed lines), subdivided into convective, stratiform, and anvil echoes. The profiles are truncated similarly to the CFADs shown in Figs. 6 and 7. The dotted lines indicate the approximate altitude of the 0°C and −20°C levels.

anvil echoes (Fig. 10c). The average uncertainty of a stratiform mean profile, for a twice-daily frequency of observation, is less than 1 dBZ up to heights of approximately 10 km. Because of its low sensitivity, however, the TRMM radar samples will likely not measure the reflectivity profile accurately above ~ 7.5 km. The data for the melting layer (bright band) and below are likely not reflecting unbiased samples either, due to attenuation.

The results obtained for period 2 are qualitatively

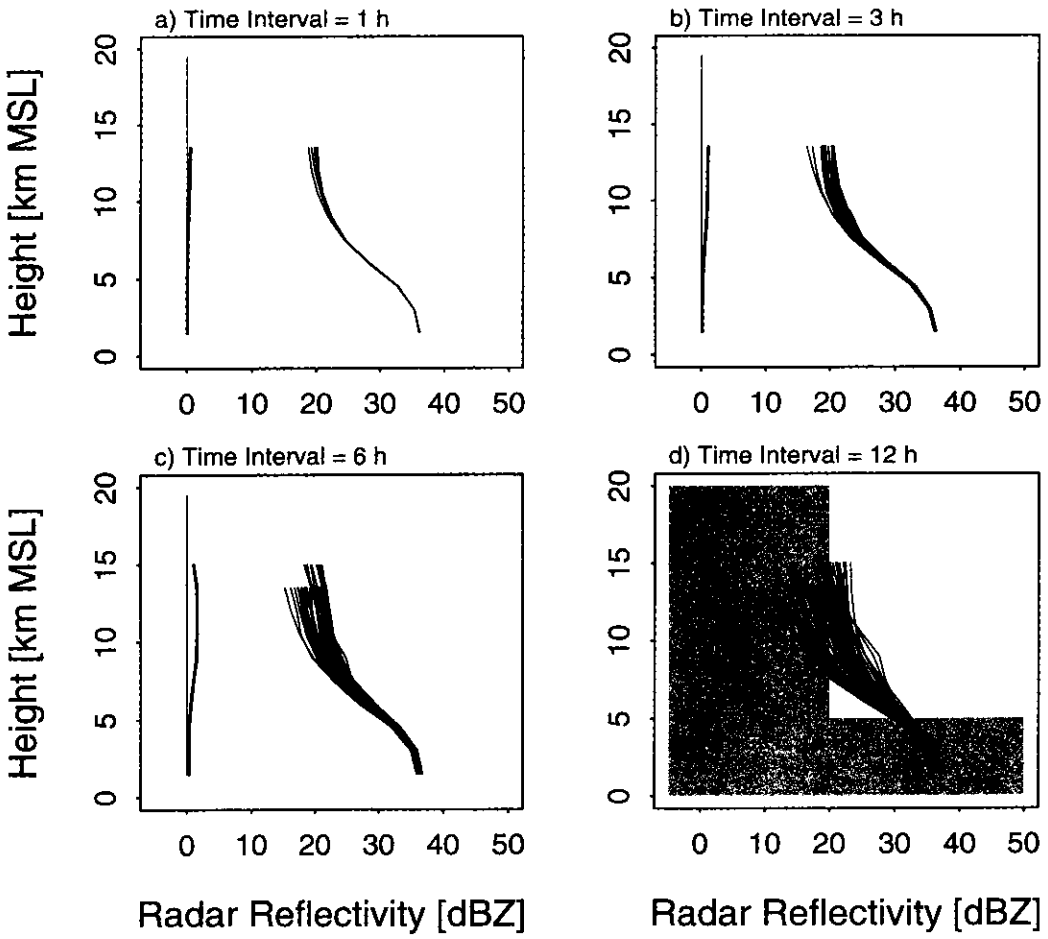

Fig. 9. Mean vertical reflectivity profiles for various subsampling frequencies of radar volumes collected during period 1 and using the convective echoes only. For each given sampling time interval all the different realizations of estimating a monthly mean profile are shown. a) $\Delta t = 1$ h, b) $\Delta t = 3$ h, c) $\Delta t = 6$ h, and d) $\Delta t = 12$ h. Each mean profile is individually truncated similarly as pointed out for the CFADs shown in Fig. 6. To the left of the mean profiles, the standard deviation (computed using reflectivity in linear units, but expressed again in logarithmic units) of the different mean profile reflectivity values obtained at each altitude is indicated. The shaded area outlined in Fig. 9d indicates the range of values affected by the TRMM precipitation radar sensitivity (approximately 20 dBZ) and signal attenuation (below the 0°C level at about 5 km).

very similar to those of period 1, except that the uncertainties increase less rapidly with decreasing sampling frequency and altitude of observation (*cf.*, Figs. 10b and 11). The reason for this difference in magnitude of the sampling uncertainty between period 1 and period 2 can be attributed to differences of the rainfall characteristics for the two periods. The areal rainfall accumulation was higher in period 2, which exhibits the smaller sampling uncertainties than period 1. It appears, therefore, that the uncertainty of monthly mean reflectivity profiles may be characterized by similar scaling rules as for areal rainfall amounts (Bell *et al.*, 1990, 1996; Steiner, 1996; and references therein).

Several important characteristics of precipitation are empirically related to the radar reflectivity Z by a relationship of the form

$$X = \gamma Z^{\delta} \tag{2}$$

where X may be the rainfall rate or liquid water content (snowfall intensity or ice water content above the 0°C level), γ and δ are positive constants, and $0 \leq \delta \leq 1$. Using relation (2) to convert Z to X, an uncertainty in Z (*i.e.*, ΔZ) causes an uncertainty in X (*i.e.*, ΔX). This uncertainty of the quantity X, expressed as

$$\frac{\Delta X}{X} = \frac{X(Z+\Delta Z) - X(Z-\Delta Z)}{2X(Z)} \cdot 100\ \% = \frac{(Z+\Delta Z)^{\delta} - (Z-\Delta Z)^{\delta}}{2Z^{\delta}} \cdot 100\ \% \tag{3}$$

is shown in Fig. 12 (in contours) as a function of ΔZ and the power factor δ. The light shaded area indicates the likely range of power factors of relationships found in the literature for rain, while the

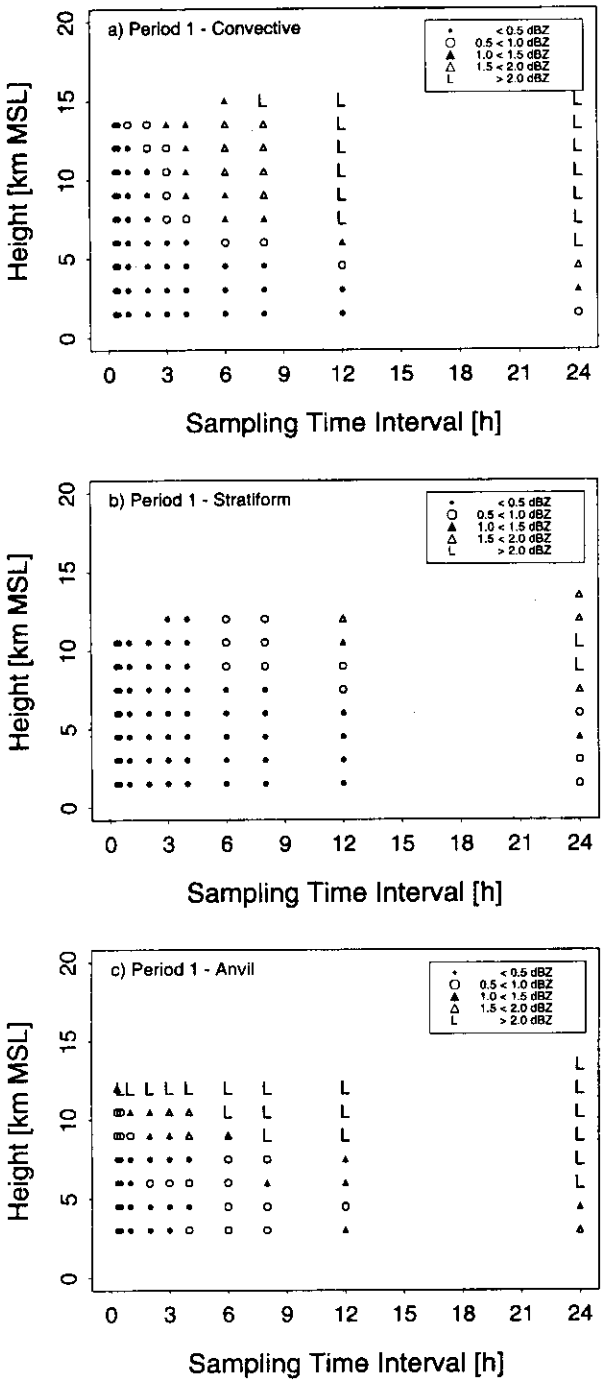

Fig. 10. Standard deviation of monthly mean reflectivity estimates as a function of height and frequency of observation based on radar data collected during period 1 for a) convective, b) stratiform, and c) anvil echoes.

heavy shaded area shows the respective range for snow (*e.g.*, Battan, 1973). For a TRMM-like configuration (*i.e.*, sampling approximately twice daily) and rainfall as observed in the monsoonal regime at Darwin, the uncertainty of monthly mean reflectivity values caused by infrequent sampling may be of

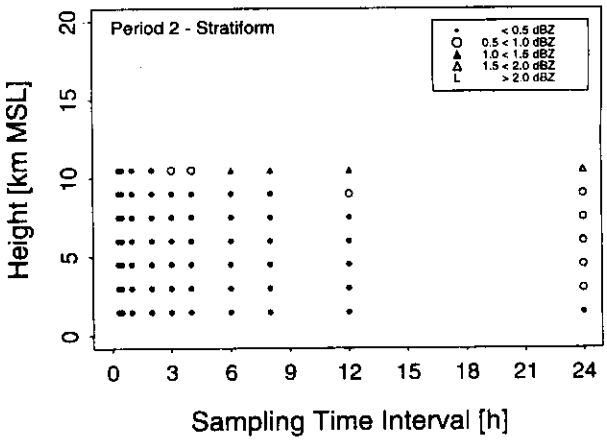

Fig. 11. Same as Fig. 10b, except for radar data collected during period 2.

the order of ±1.5 dBZ in the rain and ±2 dBZ (or larger) in the ice (Figs. 9–11). According to Fig. 12, the sampling-related uncertainty of the derived quantity X, on the average, could therefore be as large as 20 %, both within rain and snow. In addition, this value may likely be larger due to uncertainties in the selection of the parameters γ and δ.

4. Surface rainfall

This section analyzes the effects of a reduced frequency of observation on the accuracy of surface rainfall estimates, in particular the areal mean rainfall accumulation, convective fraction, and spatial distribution.

4.1 Accuracy of monthly areal mean rainfall

We use every radar volume scan collected during period 1 to calculate an areal rainfall of 245 mm over an area within a radius of 150 km of Darwin (Fig. 3a, Table 1). If we were to use only one radar observation per day, always taken at the same time, and estimate the monthly rainfall based on just those samples selected, we obtain a different estimate. This estimate, moreover, depends on what time of day the observations were taken. If we plot the different estimates as a function of the time of day the samples were collected, we obtain the diurnal cycle of the areal rainfall, as shown in Fig. 13. The bold horizontal line at 245 mm represents the areal rainfall accumulation based on all the available samples, while the other curves are estimates based on only one sample per day. The solid curve with dots indicates the diurnal rainfall signature obtained by using the entire area-wide information, while the dotted and dashed lines reflect the diurnal cycle of rainfall over land and ocean, respectively. Figure 14 shows the diurnal rainfall signature over land decomposed into a diurnal cycle of the islands to the north of

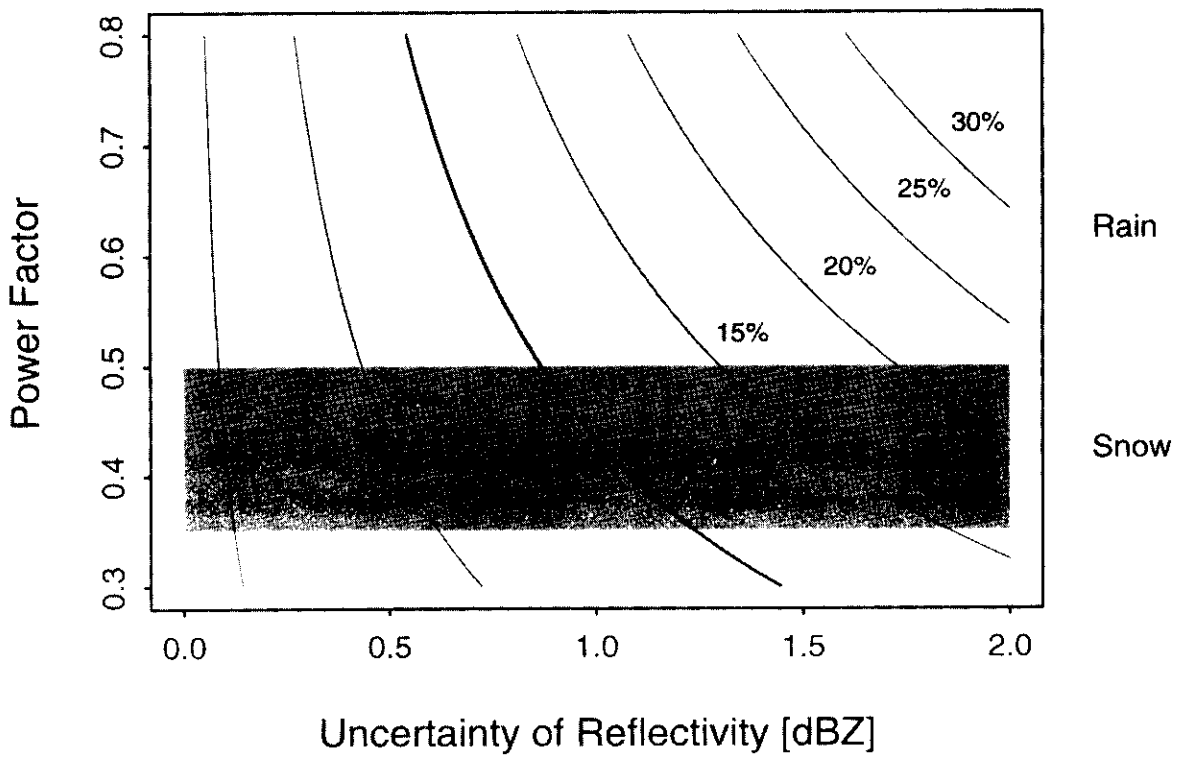

Fig. 12. Relative error of precipitation quantities (in contours) derived from empirical reflectivity-based power-law relationships as a function of the uncertainty of the reflectivity observation and the power factor of the relationship used. The shaded areas indicate the likely range for power factors of relationships found in the literature for rain and snow. See text for details.

Darwin (peak near 1500 LST)[8] and the remaining continent (peak at approximately 2200 LST). The oceanic peak in rainfall lags the nocturnal continental peak by about 3–6 hours. These results are consistent with those of Keenan *et al.* (1988, 1989b, 1990), Steiner *et al.* (1995), and Li *et al.* (1996).

Full resolution in time (every radar volume) versus only one sample per day (always taken at a particular time of day) represent two extreme cases. The latter case results in the largest uncertainty of the monthly areal mean rainfall estimate compared to the value given by incorporating all the data into the analysis. Figure 15a summarizes the results obtained for period 1 by varying the sampling frequency from one to the other extreme. This type of plot was introduced by Steiner *et al.* (1995). At the sampling time interval of $\Delta t = 24$ h (one sample per day), the different estimates range from 100 mm to over 400 mm (same as in Fig. 13). By decreasing Δt to 12 h, the spread of these values is reduced to a range of 180–320 mm, and any further decrease of Δt reduces the range of estimates. The spread of the different estimates of areal rainfall accumulation for a given sampling frequency is a measure of the uncertainty to be expected, on the average, for any estimate at that particular frequency of observations. This uncertainty is quantified by the standard deviation of the different estimates for a given sampling frequency and is shown in Fig. 15a by the heavily (lightly) shaded bars indicating the mean plus/minus one (two) standard deviation(s). The increase in uncertainty of the areal mean rainfall estimate as a function of decreasing sampling frequency is approximated by the sloping dashed line (indicating an average uncertainty increase of 1.5 % per hour decrease in sampling frequency), which embraces the mean plus/minus one standard deviation for the various sampling frequencies. The dotted horizontal lines show where the uncertainty reaches 50 % of the areal mean rainfall based on all the available samples.

Figure 15b presents the results corresponding to Fig. 15a but based on the radar data collected during period 2. The areal mean rainfall was 374 mm for this period, compared to 245 mm in period 1, and the sampling-related uncertainties are significantly smaller than for period 1. This can be seen, for example, by the sloping dashed line in Fig. 15b, which represents the envelope characterizing the average uncertainty to be expected as a function of the sampling frequency based on the data of period 1. This decrease in sampling uncertainty with increasing rainfall amount is expected (Laughlin, 1981; North, 1988; Bell *et al.*, 1990, 1996; Graves

8 Local Standard Time (LST) for Darwin, Australia, is UTC plus 9.5 hours.

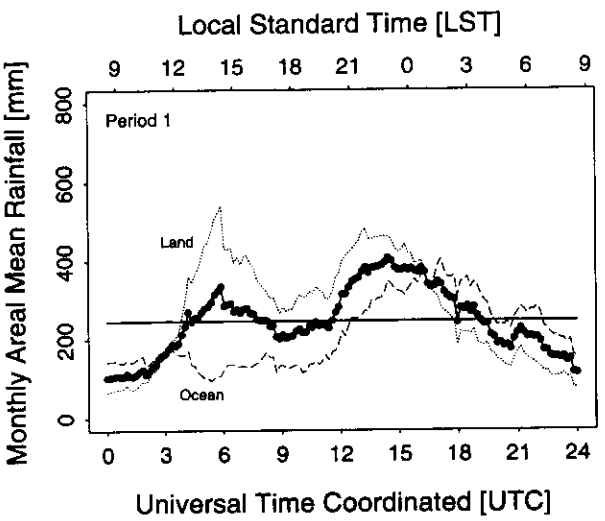

Fig. 13. Diurnal signatures for rainfall observed within a radius of 150 km around Darwin during period 1. The bold horizontal line indicates the rain gauge-adjusted areal mean rainfall accumulation for the time period. The solid curve with dots represents the areal mean diurnal rainfall cycle for the entire domain, while the dotted and dashed lines are diurnal rainfall signatures derived from using radar-rainfall echoes over land and ocean, respectively. See text for further details.

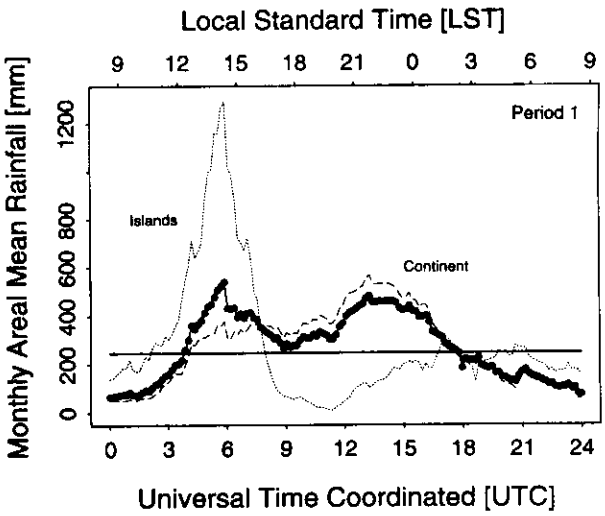

Fig. 14. Similar to Fig. 13, but the solid curve with dots represents here the diurnal rainfall signature over land (same as dotted line in Fig. 13), and the dotted and dashed lines represent the cycles decomposed into over the islands and the remaining continent.

et al., 1993; Oki and Sumi, 1994; Weng *et al.*, 1994; Bell and Kundu, 1996; Steiner, 1996; among others).

The increase in uncertainty with decreasing sampling resolution, as depicted in Fig. 15, is not necessarily linear as assumed here for simplicity reasons. It is noteworthy to point out that the Laughlin-type formula (Laughlin, 1981) like the one in equations (23) and (24) of Bell *et al.* (1990) predicts that the uncertainty should increase linearly with sampling time interval Δt for small Δts (*i.e.*, Δt small compared to the correlation time of the area-averaged rain) but that it should increase as $\Delta t^{0.5}$ for large Δt. The latter behavior is given in equation (30) of Bell *et al.* (1990). In addition, Li *et al.* (1996) used stationary and nonstationary rainfall process models to study the sampling errors associated with space-based rainfall measurements. The results from their nonstationary model showed that the sampling error is sensitive to the starting sampling time for some sampling frequencies, due to the diurnal cycle of rain, but not for others (Fig. 18 of Li *et al.*, 1996). Sampling experiments using data showed such sensitivity as well (Fig. 20 of Li *et al.*, 1996). When the errors were averaged over starting time, however, the results of the experiments and the stationary and nonstationary models matched each other very closely (Figs. 19 and 21 of Li *et al.*, 1996).

4.2 Accuracy of convective fraction of rainfall

Previous studies have not investigated the effect of sampling on the accuracy of the ratio of convective to stratiform precipitation. The fraction of the rainfall that is convective as opposed to stratiform is relevant to the vertical profile and gradient of latent heating (Houze, 1982, 1989, 1997) and thus to the TRMM objectives (Simpson *et al.*, 1988, 1996). This section investigates the effect of a reduced frequency of observations on the estimated monthly convective rain fraction.

Based on only one radar volume scan observation per day, always taken at the same time, the estimates of the monthly convective rain fraction may range from 29 % to 76 % for period 1 (34 % to 61 % for period 2). Plotted as a function of the time of day they were taken, these estimates reveal the diurnal signature depicted in Fig. 16. Over land, the maximum of the convective rain fraction is reached in the mid afternoon (dominated by the heavily convective island thunderstorms) and then slowly decreases towards the evening before it relative rapidly drops off around 2200 LST. As noted by Keenan *et al.* (1989b), the oceanic signature is significantly less pronounced, varying between 50 % and 70 % for most of the day, but shows a clear minimum during the early to mid morning hours (0300–0900 LST).

The uncertainty of the convective rain fraction estimate as a function of the frequency of observation is shown in Fig. 17 for period 1 and period 2, respectively. This figure is similar to Fig. 15 for the rainfall total. The sloping dashed lines shown in Figs. 17a and 17b indicate an uncertainty increase

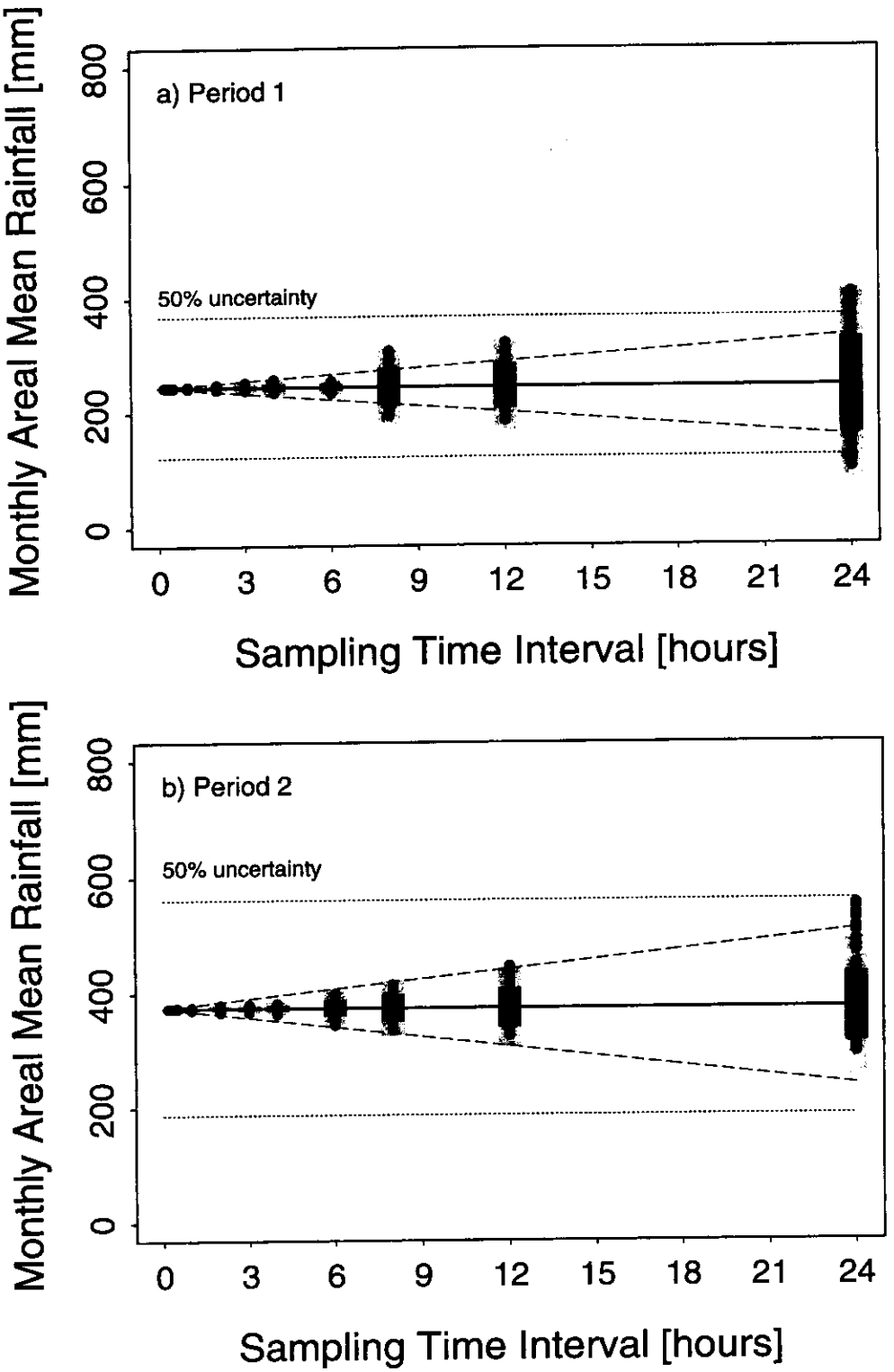

Fig. 15. a) Uncertainty of the areal rainfall as a function of sampling frequency for period 1. The heavy (light) shaded area in each sampling time interval bin corresponds to the range of mean plus/minus one (two) standard deviation(s) of all the different realizations shown by the dots. The heavy horizontal line indicates the monthly areal mean rainfall accumulation for this particular time period and site based on using all the radar volume scans collected. The 50 % uncertainty range is shown by the dotted horizontal lines. The sloping dashed lines indicate an approximate 1.5 % increase in uncertainty of the monthly areal rainfall estimate per hour decrease in sampling time resolution. b) Same as Fig. 15a, except for radar volumes collected during period 2. The average uncertainty increase as a function of sampling frequency observed for period 1 (Fig. 15a) is reproduced by the dashed sloping line.

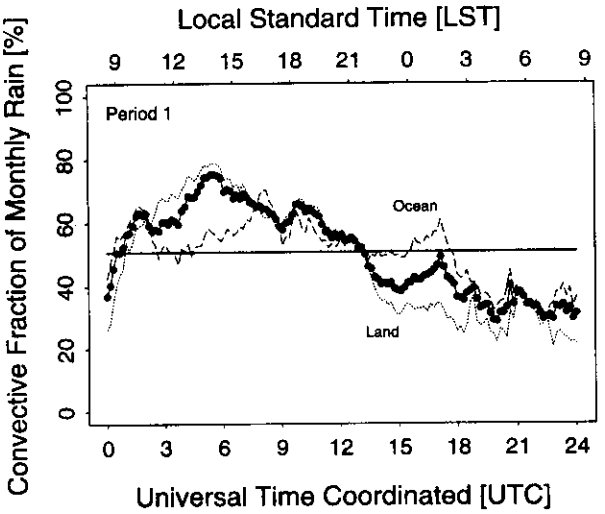

Fig. 16. Diurnal signature of the convective rain fraction for period 1, similar to Fig. 13.

of 1 % (of the monthly mean value) per hour of decrease in sampling frequency. For example, given a monthly mean convective rain fraction of 50 %, the expected uncertainty for a twice-daily sampling (estimated based on the indicated sloping dashed lines) would be 12 % (*i.e.*, ±6 %). The envelope spanned by the indicated dashed lines in Fig. 17 reflects approximately the uncertainties for period 1 (Fig. 17a), however, it overestimates those of period 2 (Fig. 17b). The sampling uncertainty for the convective rain fraction thus behaves qualitatively like that of the rainfall total. We again see an inverse dependence on the rainfall amounts, with period 2 (which accumulated much more rain) exhibiting significantly smaller uncertainties than period 1.

Ground-based radar observations indicate that the convective rain fraction may range between 30 % and 60 % (Section 2.3). Figure 17 suggests that the uncertainty of the monthly convective rain fraction for a twice-daily sampling (like the TRMM satellite) may range between 10 % and 15 % of the monthly mean, dependent on the rainfall total. Combination of this uncertainty with other uncertainties in estimating the convective rain fraction, resulting from echo classification (Steiner *et al.*, 1995) and a choice of $Z-R$ relation (Steiner and Houze, 1997), implies that the total uncertainty in the monthly convective rain fraction, and hence in the vertical profile of latent heating, will be substantial when estimated from the TRMM satellite data.

4.3 Accuracy of the spatial distribution of monthly rainfall

4.3.1 Coefficient of variation

The coefficient of variation is defined here as the standard deviation of the spatial variability of a given rainfall map divided by its areal mean accumulation, and this ratio is expressed as a percentage. The spatial variability of the monthly rainfall distribution is quite different from a variability in time, which has been investigated in studies of sampling problems of rainfall (*e.g.*, Bell *et al.*, 1990; Graves *et al.*, 1993 ; Li *et al.*, 1996). The purpose of this section is to study the impact of a reduced frequency of observation on determining the spatial rainfall distribution on a monthly basis; the coefficient of variation is used as a measure to quantify the spatial variability.

Figures 18a and 18b demonstrate the effect of subsampling on the coefficient of variation for period 1 and 2, respectively. The coefficients of variation obtained for period 1 and 2 using full time resolution (*i.e.*, radar volume scan every 10 min) are 30 % and 34 %, respectively. Figure 18 shows a clear trend towards an increase in the estimated coefficient of variation (spatial variability) with decreasing sampling frequency. The dotted horizontal line in Figs. 18a and 18b indicates a spatial variability that is twice as large as the one obtained by using full time resolution. For period 2, where significantly more rainfall was accumulated, that doubling of the estimated spatial variability of the monthly rainfall map is reached, on the average (solid line), at a subsampling rate of one observation every 6 h, while for the less rainy period 1 that level is reached after only 3 h. Thus, we again see that sampling-related behavior being sensitive to the total amount of rain.

4.3.2 Correlation

Another measure of the effect of subsampling on the spatial distribution of rainfall is the correlation of the subsampled rain maps with maps based on all the radar samples. The correlation is computed on the basis of a pixel by pixel comparison for the entire 2-km gridded domain between the full resolution rainfall map ($Rfull$) and the one produced by subsampling (R_{subs}) using the following expression

$$\begin{aligned} correlation = & \sum_{i,j}^{N} \left\{ \left(R_{full}(i,j) - \frac{1}{N} \sum_{i,j}^{N} R_{full}(i,j) \right) \cdot \right. \\ & \left. \left(R_{subs}(i,j) - \frac{1}{N} \sum_{i,j}^{N} R_{subs}(i,j) \right) \right\} \Bigg/ \\ & \left\{ \sqrt{\sum_{i,j}^{N} \left(R_{full}(i,j) - \frac{1}{N} \sum_{i,j}^{N} R_{full}(i,j) \right)^2} \right. \\ & \left. \sqrt{\sum_{i,j}^{N} \left(R_{subs}(i,j) - \frac{1}{N} \sum_{i,j}^{N} R_{subs}(i,j) \right)^2} \right\} \end{aligned} \tag{4}$$

where i and j are indices indicating the position

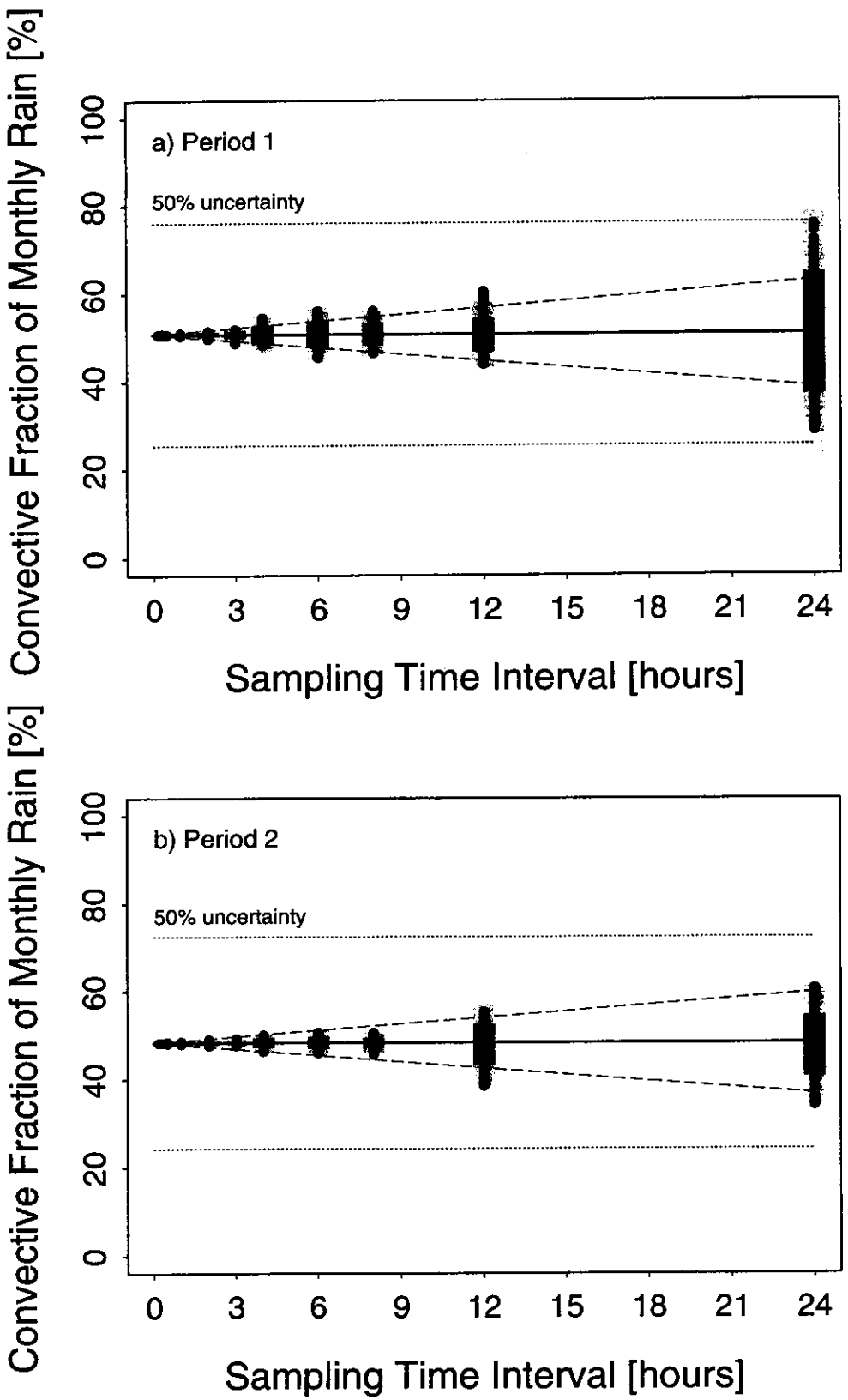

Fig. 17. Uncertainty of the convective rain fraction as a function of sampling frequency for a) period 1 and b) period 2, similar to Fig. 15. The sloping dashed lines indicate an approximate 1 % increase in uncertainty of the monthly convective rain fraction estimate per hour decrease in sampling time resolution.

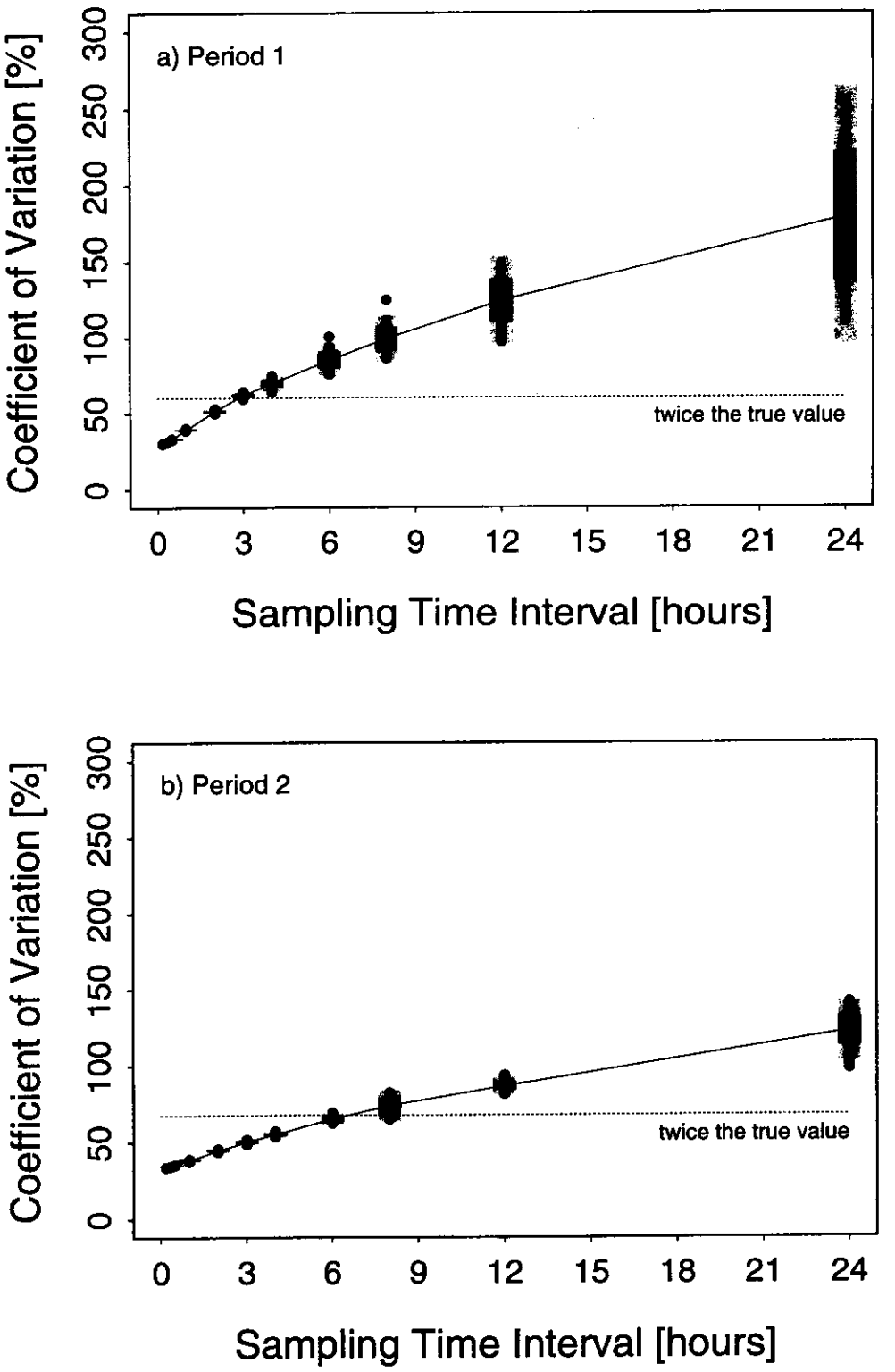

Fig. 18. Spatial variability of the monthly rainfall distribution, expressed by the coefficient of variation, as a function of the sampling frequency. The results are based on the radar data collected at Darwin during a) period 1 and b) period 2. The dots shown at a particular sampling frequency indicate the different estimates obtained for every different subsampling realization. The heavy (light) shading indicates the mean plus/minus one (two) standard deviation(s) of those estimates. The solid line connects the mean estimate of the coefficient of variation for different sampling frequencies. The dotted horizontal line indicates a coefficient of variation twice as large as the value obtained using full time resolution.

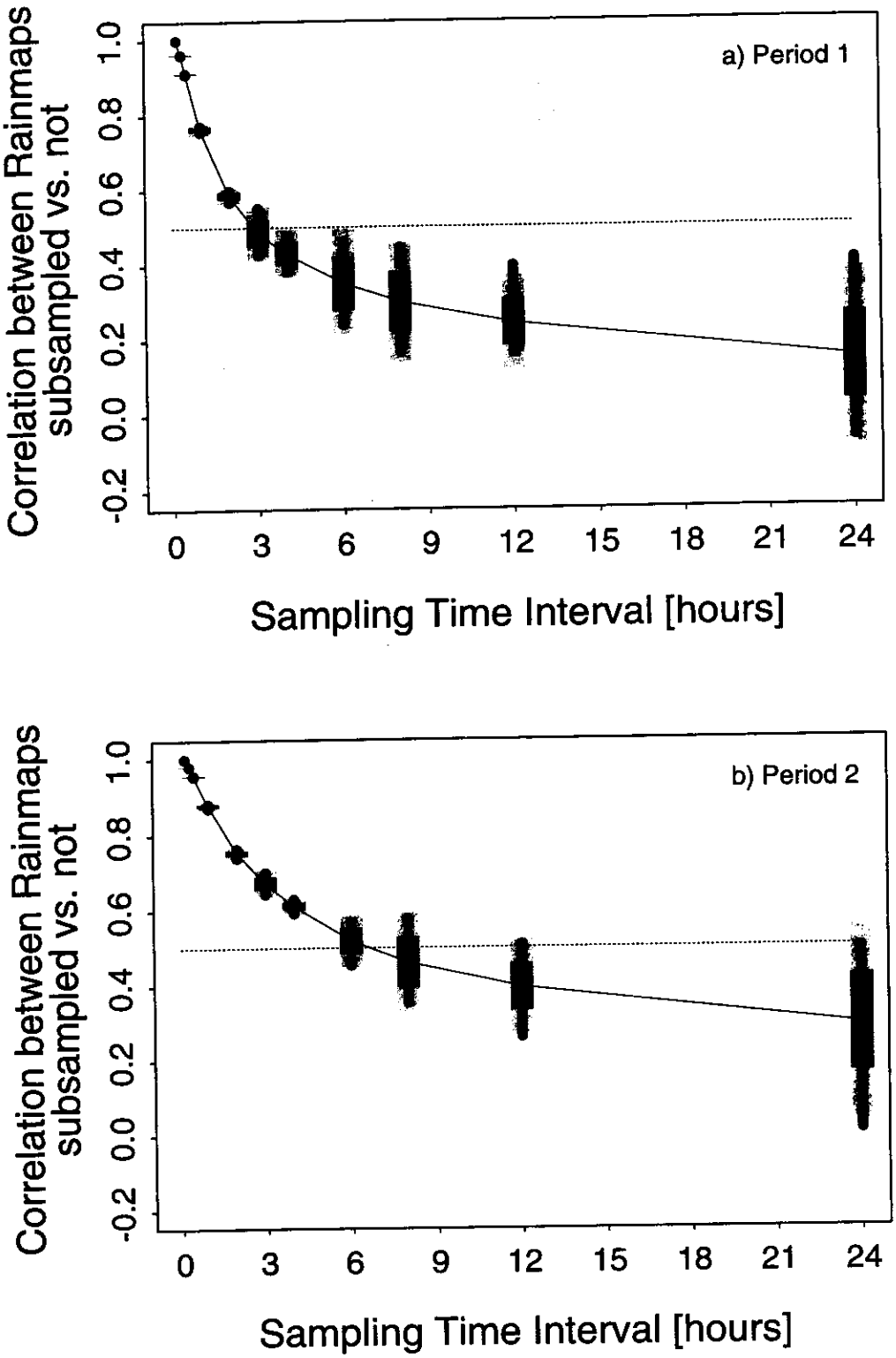

Fig. 19. Correlation (on a pixel by pixel basis) between the subsampled and full time resolution rainfall maps as a function of the sampling frequency. The results are based on the radar data collected at Darwin during a) period 1 and b) period 2. The dots shown at a particular sampling frequency indicate the different estimates obtained for every different subsampling realization. The heavy (light) shading indicates the mean plus/minus one (two) standard deviation(s) of those estimates. The solid line connects the mean estimate of the correlation for different sampling frequencies. The dotted horizontal line indicates a correlation of 0.5.

within a given rainfall map. For each subsampling time interval (Δt) all the different realizations (starting at different times of day) are calculated and plotted in Fig. 19a as a function of Δt. The solid curve indicates the mean of the different correlation estimates, while the heavily (lightly) shaded bars show the range of mean plus/minus one (two) standard deviation(s). For period 1, the correlation between the full resolution and subsampled rainfall maps decreases rapidly with increasing Δt. For example, the monthly spatial rainfall distribution derived from rain maps at a sampling interval of $\Delta t = 1$ h shows a correlation of 0.75 to the 10-min (full resolution) rainfall accumulation. At $\Delta = 3$ h, the correlation between the true and the subsampled rain maps is only 0.5 (dotted line). The correlation does not drop off quite as dramatically for period 2 (Fig. 19b), which exhibited significantly more rainfall, thus suggesting again a scaling with rainfall amount.

These results imply that the monthly spatial rainfall distribution derived from the TRMM satellite (approximately two observations daily) will show little correlation with the true rainfall map, for example, the map obtained by ground-based radar observations taken at high temporal resolution. However, the correlation between the subsampled and full resolution rain maps depends on the horizontal grid resolution of the maps as well. The drop off in correlation is reduced not only with increasing rain amount but also with decreasing resolution of the rain map. The goal of the TRMM satellite is to obtain accurate monthly mean rain estimates over 500 km by 500 km areas (Simpson *et al.*, 1988, 1996); it is not to produce detailed spatial patterns on the monthly time scale. The TRMM ground validation radars will, however, provide monthly data at a high time resolution ($\Delta t \leq 30$ min). Figures 18 and 19 suggest that the monthly rain maps based on the ground validation site data will be useful.

5. Conclusions

Spaceborne radar (such as that on the TRMM satellite) aims to obtain accurate monthly three-dimensional characteristics of precipitation. Since the TRMM satellite revisits a 500 km by 500 km region only about twice a day, and since precipitation is highly intermittent in time and space, the question arises, how accurate are the satellite-based monthly precipitation data? The focus of this investigation has been on monthly representations of the vertical structure of the radar reflectivity of precipitation systems, the surface rainfall (areal mean as well as the spatial distribution), and the partitioning of the radar echoes into convective, stratiform, and anvil (no surface rainfall) components, all of which are important to a climatological assessment of the latent heating of the tropical atmosphere. Uncertainties in these monthly representations as a function of the frequency of sampling have been estimated by comparing the results based on subsampling to those obtained by using all of the available observations. Radar and rain gauge data collected at Darwin, Australia, during the 1993/94 rainy season have been used for this study.

Monsoon and break periods in the Darwin precipitation regime can be recognized in both the vertical structure products (reflectivity CFAD and mean profiles) and the echo area statistics. Months with a significant rainfall contribution by break (continental) precipitation systems tend to show higher reflectivities aloft than does oceanic rainfall. The intense island thunderstorms ("Hectors"), which occurred regularly during break periods in the Australian monsoon over the islands to the north of Darwin, can be recognized in the echo area statistics and diurnal rainfall signatures.

The subsampling analyses revealed the expected trend that the uncertainties of estimated precipitation characteristics using infrequent observations scale with rainfall amount for all the variables investigated; the sampling-related uncertainties are smaller for months with higher rainfall amounts. While for areal mean rainfall the sampling behavior is relatively well understood (*e.g.*, Bell *et al.*, 1990, 1996; Bell and Kundu, 1996; Steiner, 1996; and references listed therein), the present study indicates the need to explore further the sampling uncertainties with regard to the horizontal and vertical structure of precipitation.

This study shows that the uncertainty of monthly mean reflectivity values increases with increasing altitude (and decreasing number of data) and with decreasing temporal sampling frequency. The uncertainty of the monthly mean reflectivity profile increases much more rapidly with decreasing frequency of observation above the 0°C level than below within the rain. The TRMM satellite will sample a 500 km by 500 km region about twice daily. At a 12 h sampling interval, on the average, the uncertainty in the monthly mean reflectivity profile is about ±1.5 dBZ below the 0°C level (in rain) and ±2 dBZ above the 0°C level (in snow). In addition to this difficulty, the radar signal of the TRMM satellite will be highly attenuated below the 0°C level, and the TRMM satellite radar will be insensitive to reflectivity less than about 20 dBZ. Because of these limitations, the only altitude range in which the TRMM radar may give reliable reflectivity statistics is between about 5 and 7.5 km (Fig. 9d). Within this altitude range, however, mixed-phase precipitation processes take place that are very important for cloud electrification.

Because of differences in vertical structure and intensity, however, the uncertainties and caveats pointed out above may vary between convective and

stratiform precipitation and anvil echoes. The uncertainties in reflectivity tend to be larger for the convective mean profiles than those composed of stratiform echoes. The stratiform regions do not show much variation from one region to another. This result is consistent with Houze's (1989) suggestion that the greatest uncertainty in precipitating cloud systems in the tropics is in the vertical structure of the convective echo regions. Nonetheless, the TRMM satellite radar will obtain an obscured picture of the vertical precipitation structure. Classification algorithms based on using TRMM satellite radar data should therefore incorporate horizontal precipitation structure as well, rather than rely on vertical structure information alone.

The vertical gradient of heating in the tropics is sensitive to the convective rain fraction. This study shows that the convective rain fraction for Darwin would be uncertain up to ± 10 % if sampled only two times per day. Combination of this uncertainty with other uncertainties in estimating the convective rain fraction, for example, resulting from echo classification (Steiner *et al.*, 1995) and a choice of $Z - R$ relation (Steiner and Houze, 1997), indicates that the uncertainty in the derived vertical gradient of latent heating will be substantial when estimated from TRMM satellite data only. This result means that the ground validation radars in TRMM, which sample about every 10 min and with high sensitivity, must be used to improve upon TRMM satellite estimates of the convective rain fraction.

The horizontal rainfall distribution is very sensitive to sampling frequency. Subsampling significantly increases the difference between estimated and the true rainfall distribution (*i.e.*, that based on continuous observations). The correlation between a subsampled rainfall map and the map based on all available radar observations drops rapidly with decreasing sampling frequency; for example, at Darwin the 2-km resolution monthly rainfall maps become meaningless if precipitation is sampled at 1–3 h intervals or less frequently. This decrease in correlation (or increase of spatial variability) scales with rainfall amount and with the horizontal resolution of the rainfall maps.

Overall, the results of this study suggest that the TRMM satellite radar data will be useful only with certain restrictions. The radar echo data will be most useful in the altitude range 5–7.5 km and particularly if they are used in conjunction with more sensitive and continuously sampling ground validation site radar data. The challenge will be to retrieve quantitative information about precipitation and its three-dimensional structure over the entire depth of the troposphere, given the constraints of the TRMM satellite radar data due to instrument sensitivity and signal attenuation. This emphasizes the need for a careful treatment of the data, development of applicable attenuation correction schemes, and combining data from various sources.

Acknowledgments

The rain gauge and radar data have been provided by the TRMM Office. Stacy R. Brodzik facilitated the data management, and Joseph Tenerelli increased the efficiency of computer code. Sandra E. Yuter provided valuable comments. The suggestions of two anonymous reviewers have been greatly appreciated. The manuscript has been carefully proofread by Mary D. Stoner. This work was supported by NASA grant NAG 5-1599 to the University of Washington and in part by NSF grant EAR-9528886 to Princeton University.

References

Austin, P.M., 1987: Relation between measured radar reflectivity and surface rainfall. *Mon. Wea. Rev.*, **115**, 1053–1070.

Austin, P.M., S.G. Geotis, J.R. Cunning, J.L. Thomas, R.I. Sax and J.R. Gillespie, 1976: Raindrop size distributions and $Z - R$ relationship for GATE. *10th Tech. Conf. on Hurricanes and Tropical Meteorology*, Charlottesville, Virginia, Amer. Meteor. Soc.

Battan, L.J., 1973: *Radar Observation of the Atmosphere*. The University of Chicago Press, 324 pp.

Bell, T.L. and P.K. Kundu, 1996: A study of the sampling error in satellite rainfall estimates using optimal averaging of data and a stochastic model. *J. Climate*, **9**, 1251–1268.

Bell, T.L., A. Abdullah, R.L. Martin and G.R. North, 1990: Sampling errors for satellite-derived tropical rainfall: Monte Carlo study using a space-time stochastic model. *J. Geophys. Res.*, **95**, 2195–2205.

Bell, T.L., P.K. Kundu and C. Kummerow, 1996: Sampling error of satellite estimates of gridded rainfall. *Proc., 13th Conference on Probability and Statistic in the Atmospheric Sciences*, San Francisco, California, Amer. Meteor. Soc., 296–300.

Cheng, C.-P. and R.A. Houze Jr., 1979: The distribution of convective and mesoscale precipitation in GATE radar echo patterns. *Mon. Wea. Rev.*, **107**, 1370–1381.

Chong, M. and D. Hauser, 1989: A tropical squall line observed during the COPT 81 experiment in West Africa. Part II: Water budget. *Mon. Wea. Rev.*, **117**, 728–744.

Churchill, D.D. and R.A. Houze Jr., 1984: Development and structure of winter monsoon cloud clusters on 10 December 1978. *J. Atmos. Sci.*, **41**, 933–960.

Donaldson, R.J., Jr., 1964: A demonstration of antenna beam errors in radar reflectivity patterns. *J. Appl. Meteor.*, **3**, 611–623.

Drosdowsky, W., 1984: Structure of a northern Australian squall line system. *Aust. Met. Mag.*, **32**, 177–183.

Drosdowsky, W., 1996: Variability of the Australian summer monsoon at Darwin: 1957–1992. *J. Climate*, **9**, 85–96.

Fabry, F., G.L. Austin and D. Tees, 1992: The accuracy of rainfall estimates by radar as a function of range. *Quart. J. Roy. Meteor. Soc.*, **118**, 435–453.

Gage, K.S., C.R. Williams and W.L. Ecklund, 1994: UHF wind profilers: A new tool for diagnosing tropical convective cloud systems. *Bull. Amer. Meteor. Soc.*, **75**, 2289–2294.

Gamache, J.F. and R.A. Houze Jr., 1983: Water budget of a mesoscale convective system in the tropics. *J. Atmos. Sci.*, **40**, 1835–1850.

Graves, C.E., J.B. Valdés, S.S.P. Shen and G.R. North, 1993: Evaluation of sampling errors of precipitation from spaceborne and ground sensors. *J. Appl. Meteor.*, **32**, 374–385.

Holland, G.J., 1986: Interannual variability of the Australian summer monsoon at Darwin: 1952–82. *Mon. Wea. Rev.*, **114**, 594–604.

Houghton, H.G., 1968: On precipitation mechanisms and their artificial modification. *J. Appl. Meteor.*, **7**, 851–859.

Houze, R.A., Jr., 1977: Structure and dynamics of a tropical squall-line system. *Mon. Wea. Rev.*, **105**, 1540–1567.

Houze, R.A., Jr., 1982: Cloud clusters and large-scale vertical motions in the tropics. *J. Meteor. Soc. Japan*, **60**, 396–410.

Houze, R.A., Jr., 1989: Observed structure of mesoscale convective systems and implications for large-scale heating. *Quart. J. Roy. Meteor. Soc.*, **115**, 425–461.

Houze, R.A., Jr., 1993: *Cloud Dynamics*. Academic Press, San Diego, 573 pp.

Houze, R.A., Jr., 1997: Stratiform precipitation in regions of convection: A meteorological paradox? *Bull. Amer. Meteor. Soc.*, **78**, 2179–2196.

Houze, R.A., Jr. and E.N. Rappaport, 1984: Air motions and precipitation structure of an early summer squall line over the eastern tropical Atlantic. *J. Atmos. Sci.*, **41**, 553–574.

Hudlow, M., 1979: Mean rainfall patterns for the three phases of GATE. *J. Appl. Meteor.*, **18**, 1656–1669.

Joss, J. and A. Waldvogel, 1990: Precipitation measurements and hydrology. In *Radar in Meteorology*, D. Atlas, Ed., Amer. Meteor. Soc., Boston, 577–606.

Keenan, T.D. and R.E. Carbone, 1992: A preliminary morphology of precipitation systems in tropical northern Australia. *Quart. J. Roy. Meteor. Soc.*, **118**, 283–326.

Keenan, T.D., G.J. Holland, M.J. Manton and J. Simpson, 1988: TRMM ground truth in a monsoon environment: Darwin, Australia. *Aust. Met. Mag.*, **36**, 81–90.

Keenan, T.D., B.R. Morton, M.J. Manton and G.J. Holland, 1989a: The Island Thunderstorm Experiment (ITEX)—a study of tropical thunderstorms in the maritime continent. *Bull. Amer. Meteor. Soc.*, **70**, 152–159.

Keenan, T.D., J. McBride, G. Holland, N. Davidson and B. Gunn, 1989b: Diurnal variations during the Australian Monsoon Experiment (AMEX) Phase II. *Mon. Wea. Rev.*, **117**, 2535–2552.

Keenan, T.D., B.R. Morton, X.S. Zhang and K. Nyguen, 1990: Some characteristics of thunderstorms over Bathurst and Melville Islands near Darwin, Australia. *Quart. J. Roy. Meteor. Soc.*, **116**, 1153–1172.

Kitchen, M. and P.M. Jackson, 1993: Weather radar performance at long range—simulated and observed. *J. Appl. Meteor.*, **32**, 975–985.

Laughlin, C., 1981: On the effect of temporal sampling on the observation of mean rainfall. In *Precipitation Measurements from Space*, Workshop Report, D. Atlas and O. Thiele, Eds., NASA Goddard Space Flight Center, Greenbelt, Maryland, D5–D66.

Leary, C.A., 1984: Precipitation structure of the cloud clusters in a tropical easterly wave. *Mon. Wea. Rev.*, **112**, 313–325.

Li, Q., R.L. Bras and D. Veneziano, 1996: Analysis of Darwin rainfall data: Implications on sampling strategy. *J. Appl. Meteor.*, **35**, 372–385.

Mapes, B.E. and R.A. Houze Jr., 1992: An integrated view of the 1987 Australian monsoon and its mesoscale convective systems. Part I: Horizontal structure. *Quart. J. Roy. Meteor. Soc.*, **118**, 927–963.

Mapes, B.E. and R.A. Houze Jr., 1993: An integrated view of the 1987 Australian monsoon and its mesoscale convective systems. Part II: Vertical structure. *Quart. J. Roy. Meteor. Soc.*, **119**, 733–754.

Mohr, C.G. and R.L. Vaughan, 1979: An economical procedure for Cartesian interpolation and display of reflectivity factor data in three-dimensional space. *J. Appl. Meteor.*, **18**, 661–670.

North, G.R., 1988: Survey of sampling problems for TRMM. In *Tropical Rainfall Measurements*, J.S. Theon and N. Fugono, Eds., A. Deepak, Hampton, Virginia, 337–348.

Oki, R. and A. Sumi, 1994: Sampling simulation of TRMM rainfall estimation using radar—AMeDAS composites. *J. Appl. Meteor.*, **33**, 1597–1608.

Ramage, C.S., 1968: Role of a tropical "maritime continent" in the atmospheric circulation. *Mon. Wea. Rev.*, **96**, 365–370.

Rosenfeld, D., D. Atlas, D.B. Wolff and E. Amitai, 1992: Beamwidth effects on $Z-R$ relations and area-integrated rainfall. *J. Appl. Meteor.*, **31**, 454–464.

Rosenfeld, D., D.B. Wolff and D. Atlas, 1993: General probability-matched relations between radar reflectivity and rain rate. *J. Appl. Meteor.*, **32**, 50–72.

Rutledge, S.A., E.R. Williams and T.D. Keenan, 1992: The Down Under Doppler and Electricity Experiment (DUNDEE): Overview and preliminary results. *Bull. Amer. Meteor. Soc.*, **73**, 3–16.

Short, D.A., D.B. Wolff, D. Rosenfeld and D. Atlas, 1993: A study of the threshold method utilizing raingage data. *J. Appl. Meteor.*, **32**, 1379–1387.

Simpson, J., R.F. Adler and G.R. North, 1988: A proposed Tropical Rainfall Measuring Mission (TRMM) satellite. *Bull. Amer. Meteor. Soc.*, **69**, 278–295.

Simpson, J., T.D. Keenan, B. Ferrier, R.H. Simpson and G.J. Holland, 1993: Cumulus mergers in the maritime continent region. *Meteor. Atmos. Phys.*, **51**, 73–99.

Simpson, J., C. Kummerow, W.-K. Tao and R.F. Adler, 1996: On the Tropical Rainfall Measuring Mission (TRMM). *Meteorol. Atmos. Phys.*, **60**, 19–36.

Smith, J.A., D.-J. Seo, M.L. Baeck and M.D. Hudlow, 1996: An intercomparison study of NEXRAD precipitation estimates. *Water Resour. Res.*, **32**, 2035–2045.

Smith, P.L., 1990: Precipitation measurements and hydrology: Panel report. In *Radar in Meteorology*, D. Atlas, Ed., Amer. Meteor. Soc., Boston, 607–618.

Steiner, M., 1996: Uncertainty of estimates of monthly areal rainfall for temporally sparse remote observations. *Water Resour. Res.*, **32**, 373–388.

Steiner, M. and R.A. Houze Jr., 1997: Sensitivity of the estimated monthly convective rain fraction to the choice of $Z-R$ relation. *J. Appl. Meteor.*, **36**, 452–462.

Steiner, M., R.A. Houze Jr. and S.E. Yuter, 1995: Climatological characterization of three-dimensional storm structure from operational radar and rain gauge data. *J. Appl. Meteor.*, **34**, 1978–2007.

Troup, A.J., 1961: Variations in upper tropospheric flow associated with the onset of the Australian summer monsoon. *Indian J. Meteor. Geophys.*, **12**, 217–230.

Wei, T. and R.A. Houze Jr., 1987: The GATE squall line of 9–10 August 1974. *Adv. Atmos. Sci.*, **4**, 85–92.

Weng, F., R.R. Ferraro and N.C. Grody, 1994: Global precipitation estimations using Defense Meteorological Satellite Program F10 and F11 special sensor microwave imager data. *J. Geophys. Res.*, **99**, 14493–14502.

Williams, E.R., S.A. Rutledge, S.G. Geotis, N. Renno, E. Rasmussen and T. Rickenbach, 1992: A radar and electrical study of tropical "hot towers." *J. Atmos. Sci.*, **49**, 1386–1395.

Wilson, J.W. and E.A. Brandes, 1979: Radar measurement of rainfall—a summary. *Bull. Amer. Meteor. Soc.*, **60**, 1048–1058.

Yuter, S.E. and R.A. Houze Jr., 1995: Three-dimensional kinematic and microphysical evolution of Florida cumulonimbus. Part II: Frequency distributions of vertical velocity, reflectivity and differential reflectivity. *Mon. Wea. Rev.*, **123**, 1941–1963.

Zawadzki, I., 1984: Factors affecting the precision of radar measurements of rain. Preprints, *22nd Conference on Radar Meteorology*, Zurich, Switzerland, Amer. Meteor. Soc., 251–256.

サンプリング頻度に対する三次元レーダーエコーの月平均特性の感度

Matthias Steiner[1] **・ Robert A. Houze Jr.**

（ワシントン大学大気科学科）

時間的に粗い観測に基づく降雨特性の評価には降雨の時空間的な変動によるあいまいさを伴う。この研究では、サンプリング頻度に依存した月平均レーダー反射強度のプロファイルと地上雨量分布の不確かさについて評価する。オーストラリア、ダーウィンにおいて1993年の終わりから1994年の春までのモンスーン期間に得られたレーダーデータと雨量計データを用いて、観測頻度に対する月平均の三次元レーダーエコーと降水特性の感度を示す。観測データは、エコーの水平及び鉛直構造に基づいて、「対流性」、「層状性」と「アンビル」に分類される。解析結果は、時間間隔の長い観測データを用いた降水特性の見積りの不確かさは降雨量に比例するという期待される傾向を明かにする。このことは、回帰頻度の高い宇宙観測プラットフォームを用いた気候学的な研究に示唆を与える。

500 km × 500 km の観測範囲をほぼ2回/日の頻度で回帰する熱帯降雨観測衛星（TRMM）搭載レーダーは、熱帯のレーダー反射強度の鉛直プロファイルを評価する上で重大な問題に直面する。ダーウィンにおける半径150 kmのレーダー観測に基づく月平均反射強度の統計は、雨と雪ともにサンプリング頻度に依存した、約20 %の不確かさを示す。また、TRMM衛星のレーダー信号は0°C層以下で強い減衰を受け、降雨レーダーでは20 dBZ以下の反射強度は測定できないであろう。それゆえ、衛星搭載レーダーでは降水の鉛直構造の観測において不明瞭な部分が残る。TRMM衛星データに基づく信頼できる反射強度の統計は、地上高度5–7.5 kmの範囲に限定されると考えられるが、その高度範囲は、液相と固相両方の降水過程が起きているので、雲内の電荷発生には重要である。サンプリングの不確かさ、信号の減衰及びレーダーの感度は降水タイプ毎に変化する。さらに、対流性の雨の割合の評価は、$Z-R$関係の選択と同様にエコー分類におけるあいまいさにより困難になる。これらの結果は、TRMM衛星による降水特性の評価を改良するための地上設置の検証用レーダーによって得られる情報と、それから推定される潜熱の鉛直プロファイルに関する情報の重要性を意味する。

[1]現在所属：プリンストン大学土木工学・オペレーションズリサーチ学科